Diagnostic Organometallic and Metallodendritic Materials for SO_2 Gas Detection: Reversible Binding of Sulfur Dioxide to Arylplatinum(II) Complexes

Martin Albrecht,[a] Robert A. Gossage,[a] Martin Lutz,[b] Anthony L. Spek,[b] and Gerard van Koten*[a]

Abstract: A series of square-planar platinum(II) complexes of the *N*,*C*,*N*′-terdentate-coordinating monoanionic "pincer" ligand, [PtX(4-E-2,6-{CH_2NRR'}$_2$-C_6H_2)] (X = Cl, Br, I, tolyl; R, R′ = Et, Me; E = H, OH, $OSiMe_2$-*t*Bu) has been prepared. In the presence of sulfur dioxide, these complexes spontaneously adsorb this gas to form pentacoordinated adducts. Solid-state crystal-structure analyses of the SO_2 adducts **8c** (X = I, R = R′ = Me, E = $OSiMe_2$*t*Bu) and **11** (X = Cl, R = R′ = Me, E = OH) show a square-pyramidal geometry around the metal center with SO_2 in the apical position. Most interestingly, the adduct **11** forms similar Pt–Cl···H–O hydrogen-bonded α-type networks as the corresponding SO_2-free complex **5**. The conservation of the supramolecular information (hydrogen-bonded self-assembly) throughout a reaction (SO_2 adsorption) is unprecedented in crystal engineering. Adduct formation in the solid state or in solution is fast and reversible and is indicated by a characteristic color change of the material from colorless to bright orange. Since facile methods have been developed to remove SO_2 from the adducts and to regenerate the square-planar starting complexes, these complexes fulfill several essential prerequisites of sensor materials for repeated diagnostic SO_2 detection. The platinum sensors have been found to be highly selective for sulfur dioxide and particularly sensitive for submilimolar to molar gas quantities. Their response capacity is tuneable by electronic and steric modifications of the ligand array by introduction of, for example, different substituents on the nitrogen donors. The periphery of dendrimers is shown to be an appropriate macromolecular support for anchoring the detection-active sites, thus allowing full recovery of the sensor materials for repeated use. By using this concept, metallo-dendrimers **3** and **15** have been prepared. Owing to the dendritic connectivity, these sensors are suitable for repetitive qualitative and *quantitative* detection of small amounts of SO_2.

Keywords: ligand design · metallodendrimers · platinum · sensors · sulfur dioxide

Introduction

A major environmental concern is the emission of sulfur-containing compounds during, for example, the combustion of fossil fuels, the extraction of sulfide ores, or from natural sources (e.g., volcanoes or oceanic phytoplankton).[1] In particular, sulfur dioxide (SO_2) is thought to contribute significantly to the production of smog and/or acid rain.[2] In the presence of hydrogen peroxide (H_2O_2) or (sun-) light and ozone, SO_2 rapidly oxidizes to SO_3, which spontaneously reacts with water to form sulfuric acid. Therefore, the detection (with a suitable sensor[3]), concentration and subsequent removal of even minute levels of SO_2 is evidently desirable.[4]

Since the synthesis of the first transition metal complexes of sulfur dioxide,[5] SO_2 has been shown to be a versatile ligand in inorganic and organometallic chemistry, as it can act as both a Lewis base or acid.[6] Various binding modes of sulfur dioxide to a metal center have been realized, making this ligand a very useful probe of the electronic character of a metal center. The bonding principles of sulfur dioxide to transition metals has been subject of various investigations.[7]

With transition metals of a formal d^6 or d^8 electronic configuration, the bonding of sulfur dioxide mainly originates

[a] Prof. G. van Koten, M. Albrecht, Dr. R. A. Gossage
Debye Institute, Department of Metal-Mediated Synthesis
Utrecht University, Padualaan 8
3584 CH Utrecht (The Netherlands)
Fax: (+31) 30-2523615
E-mail: g.vankoten@chem.uu.nl

[b] Dr. M. Lutz, Dr. A. L. Spek[+]
Bijvoet Center of Biomolecular Research
Department of Crystal and Structural Chemistry
Utrecht University, Padualaan 8
3584 CH Utrecht (The Netherlands)
Fax: (+31) 30-2533940
E-mail: a.l.spek@chem.uu.nl

[+] Address correspondence pertaining to crystallographic studies to this author.

Supporting information for this article is available on the WWW under http://www.wiley-vch.de/home/chemistry/

  0947-6539/00/0608-1431 $ 17.50+.50/0

from an interaction of the d_{z^2} orbital of the metal with the non-bonding 4_{a^1} orbital of SO_2. This overlap is constructive in the case of d^6 metal centers and, consequently, transition-metal-SO_2 complexes have been found in which the metal–sulfur vector is coplanar with the sulfur dioxide molecule (planar binding mode).[8] With d^8 metal centers, however, this primary interaction is unfavorable, since both the metal d_{z^2} and the ligand 4_{a^1} orbitals are filled. The resulting repulsion becomes less important upon bending of the SO_2 molecule, and a new interaction involving both the HOMO and LUMO (2_{b^1}) of sulfur dioxide with either the filled metal d_{xz} or d_{yz} orbital is possible. This theory is supported by the isolation of SO_2 complexes with a number of d^8 transition metals (Ni^{II}, Rh^{I}, Ir^{I}) that contain sulfur dioxide in a bent binding mode (i.e., the metal–sulfur vector crosses the plane formed by the sulfur dioxide molecule by an angle between 180° and 90°).[9]

It has been previously shown that platinum complexes containing the terdentate-coordinating monoanionic [2,6-$(CH_2NMe_2)_2$-C_6H_3]$^-$ (i.e., NCN) "pincer" ligand reversibly bind SO_2 gas.[10] Reversibility is generally not observed in transition-metal-SO_2 adducts,[7e, 11] but is an inherent prerequisite for the design of carrier and sensor materials. Furthermore, a characteristic color change of the platinum complexes has been observed upon coordination to SO_2. These facts, namely reversibility and macroscopic change of the materials properties, suggest that these compounds may be useful as diagnostic materials for SO_2 detection.[12, 13] Modification of the coordination sphere of the metal center by tuning the ligand properties can be applied as a methodology to optimize the (optical) response of these materials to SO_2. Fine-tuning of the system predominantly occurs through change of the electrophilicity of the metal center either by the introduction of electron-withdrawing or -releasing *para*-substituents on the aryl ring or by changing the basicity of the nitrogen donor atoms. In addition, this latter method enables the adjustment of the steric bulk in close proximity to the metal center, thus strongly influencing the accessibility of this atom to coordination.[14] On the other hand, fragments that have only a marginal effect on the binding sensitivity of the metal center to sulfur dioxide offer potential anchoring points for the attachment of the sensor to (in)organic supports. Platinum complexes containing a modified pincer ligand have been fixed onto dendritic molecules and these organometallic materials represent the first "dendrimer sensors" for toxic SO_2 gas.[12, 15]

Herein, we report on the fundamental factors that influence the formation of sulfur dioxide adducts with platinum complexes containing the NCN "pincer" skeleton (Figure 1).[16] Particularly intriguing is the response of the sensor capacity of these platinum complexes to various ligand

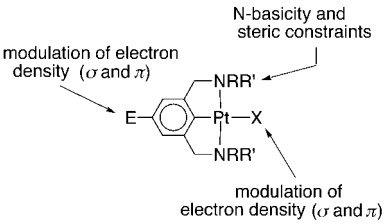

Figure 1. Potential sites for tuning the steric and electronic impact of the *N,C,N* terdentate-coordinating "pincer" ligand; this offers a suitable strategy to modify the physico-chemical properties of the metal center.

modifications (i.e., E, R, R′ and X, see Figure 1). As a result of these studies, we present arylplatinum complexes with optimized affinity of the metal center towards sulfur dioxide. Appropriate immobilization of these diagnostic sites allows the development of the first metallo-dendrimers[17] for application as fully reversible sensor materials for the selective and quantitative detection of low levels of SO_2 gas.

Results and Discussion

Synthesis: The new arylplatinum(II) complexes **2b** and **2c** were prepared following the synthetic protocol previously established for the corresponding analogues **1** (Scheme 1).[18]

Abstract in Dutch: *De synthese wordt beschreven van een reeks vlak-vierkante platina(II)-complexen, die alle een monoanionisch drietandig-gecoördineerd tangligand bevatten, [PtX(4-E-2,6-{CH_2NRR'}$_2$-C_6H_2)] (X = Cl, Br, I, tolyl; R, R′ = Et, Me; E = H, OH, $OSiMe_2tBu$). Deze complexen reageren spontaan met zwaveldioxide onder vorming van adducten met een vijf-gecoördineerd platina-centrum. Uit kristalstructuuranalyse van twee van deze adducten,* ***8c*** *(X = I, R = R′ = Me, E = $OSiMe_2tBu$) en* ***11*** *(X = Cl, R = R′ = Me, E = OH), blijkt dat SO_2 de top-positie van een vierkante pyramide bezet. Adduct* ***11*** *vormt waterstofbruggen door middel van Pt–Cl···H–O interacties; dit zelfde bindingspatroon wordt ook in het SO_2-vrije complex* ***5*** *gevonden. Dit behoud van supramoleculaire informatie (self-assemblage door waterstofbruggen) voor en na een reactie is uniek en geeft interessante mogelijkheden voor het bewerken van kristallijn materiaal (crystal engineering). De selectieve binding van SO_2 aan de platina-complexen vindt zowel in oplossing als in de vaste toestand plaats en is snel en reversibel. Bij de adsorptie van SO_2 treedt een karakteristieke kleurverandering op van kleurloos naar oranje. Zelfs zeer lage concentraties SO_2 (tot millimolaire hoeveelheden) kunnen door detectie van deze kleurverandering specifiek worden aangetoond. Milde methoden voor de verwijdering van SO_2 en het regenereren van de platina-complexen zijn ontwikkeld. Hiermee wordt aan de belangrijkste eisen voor het gebruik van deze platina-complexen als efficiënte sensormaterialen voor de detectie van SO_2 voldaan. De detectiegrens kan worden beïnvloed door het veranderen van de electronische en/of sterische eigenschappen van het tangligand (ligand tuning). Het gebruik van dendrimeren als dragermateriaal van deze SO_2 detectoren wordt beschreven. Aangezien metallodendritische macromoleculen gemakkelijk af te scheiden en terug te winnen zijn is herhaald gebruik van deze sensormaterialen voor zowel de kwalitatieve als kwantitatieve detectie van SO_2 mogelijk. Het principe van het gebruik van dendrimeren als efficiënte gas-sensoren wordt geïllustreerd met de synthese van de metallo-dendrimeren* ***3*** *en* ***15*** *en hun SO_2 adducten.*

0947-6539/00/0608-1432 $ 17.50+.50/0 *Chem. Eur. J.* **2000**, *6*, No. 8

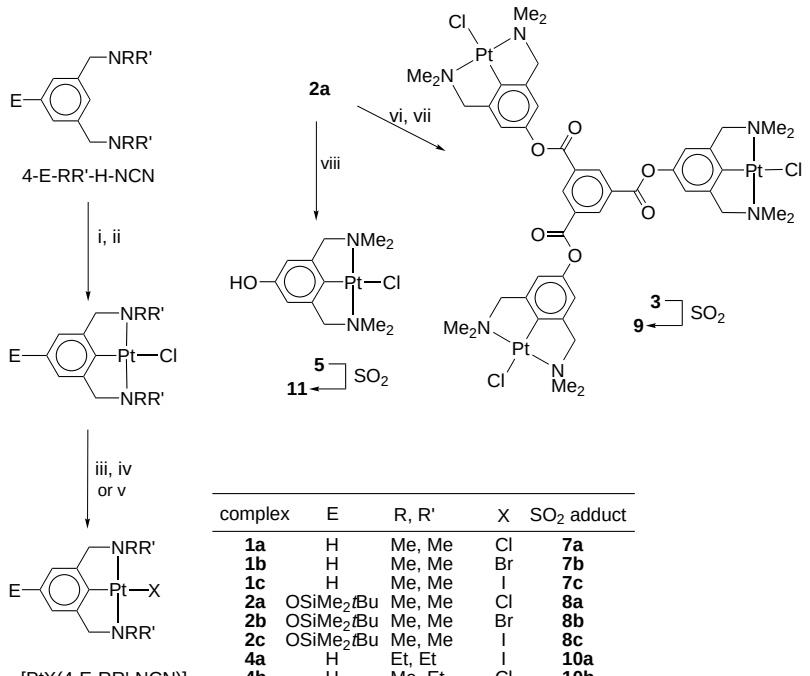

complex	E	R, R'	X	SO_2 adduct
1a	H	Me, Me	Cl	**7a**
1b	H	Me, Me	Br	**7b**
1c	H	Me, Me	I	**7c**
2a	$OSiMe_2tBu$	Me, Me	Cl	**8a**
2b	$OSiMe_2tBu$	Me, Me	Br	**8b**
2c	$OSiMe_2tBu$	Me, Me	I	**8c**
4a	H	Et, Et	I	**10a**
4b	H	Me, Et	Cl	**10b**
6	H	Me, Me	C_6H_4Me-4	**12**

Scheme 1. The synthesis of the arylplatinum(II) complexes **1**–**6**. i) *n*-BuLi, pentane; ii) $[PtCl_2(SEt_2)_2]$, Et_2O; iii) $[AgSO_3CF_3]$, acetone; iv) NaX (X = Cl, **a**; Br, **b**; I, **c**), H_2O; v) Li-C_6H_4-Me-4, Et_2O; vi) Bu_4NF, CH_2Cl_2; vii) 1,3,5-$(COCl)_3$-C_6H_3, CH_2Cl_2; viii) Bu_4NF, THF/H_2O.

Halide abstraction in [PtCl(4-$OSiMe_2tBu$-2,6-$\{CH_2NMe_2\}_2$-C_6H_2)] (**2a**, [PtCl(4-$OSiMe_2tBu$-Me,Me-NCN)]) with silver trifluoromethane sulfonate ($AgSO_3CF_3$) in wet acetone yields the cationic aqua-complex [Pt(4-$OSiMe_2tBu$-Me,Me-NCN)-(OH_2)][SO_3CF_3]. Nucleophilic substitution of the aqua ligand by a halide anion affords the corresponding neutral complexes [PtX(4-$OSiMe_2tBu$-Me,Me-NCN)] **2b** and **2c** (X = Br or I, respectively) in high yields. An asymmetric Pt^{II} complex **4b**, [PtCl(4-H-Et,Me-NCN)] was also prepared. The nitrogen centers in **4b** are stereogenic provided that Pt–N coordination occurs. Lithiation of the diaminoaryl ligand precursor 1,3-$(CH_2NEtMe)_2$-C_6H_4 afforded the 2-lithio derivative,[16b] which was subsequently transmetallated with $[PtCl_2(SEt_2)_2]$ to give **4b** as a pale-yellow air-stable solid. This compound exists as a mixture of *rac* and *meso* forms (ratio 2:3). Attempts to separate the diastereomers by column chromatography or repeated recrystallization were not successful. Prolonged heating of a toluene solution of **4b** (100 °C) does not change the *meso*:*rac* isomer distribution. This suggests either that racemization is prevented by a large kinetic barrier of the process involving reversible Pt–N bond dissociation or that the initially observed diastereomeric ratio represents the thermodynamic distribution.

The hexametallic arylester dendrimer **15** was prepared by using a convergent synthetic approach.[19] Coupling of two equivalents of **5** (as the peripheral end group) with the oxo-protected bis(acyl chloride)phenol **13** (as AB_2 branching unit)[21] yields—by double esterification—the dimetallated Pt_2 building block **14** (Scheme 2). Deprotection of the phenolic hydroxy functionality of the platinum dimer **14** and in situ esterification with the trifurcate core 1,3,5-benzenetricarboxylic acid chloride affords the hexaplatinated dendrimer **15** (first-generation dendrimer). This method is similar to the one applied for the preparation of the trimetallic complex **3** (zero-generation dendrimer).[22] Note that all difficulties associated with periphery-functionalization and end-group determination of the dendritic materials have elegantly been encompassed by using a convergent approach starting from organometallic platinum(II) building blocks. The identity of both the organoplatinum dendron **14** and the dendrimer **15** was unambiguously confirmed by elemental analysis (**14**), mass spectrometry (FAB-MS for **14**, MALDI-TOF for **15**), and ^1H and $^{13}C\{^1H\}$ NMR spectroscopy.

Adduct formation with sulfur dioxide: The exposure of the square-planar Pt^{II} complexes **1**–**6** to an atmosphere of SO_2 leads to the formation of the corresponding five-coordinate SO_2 adducts **7**–**12**. Platinum(II) centers in square-planar complexes that contain the monoanionic pincer ligand demonstrate an enhanced nucleophilicity when compared with other d^8 metal centers.[23] Consequently, they react with Lewis acids (e.g., SO_2) to form adducts. These reactions occur if the NCN-Pt complexes are in the solid state or dissolved in an appropriate solvent. Product formation is instantaneous on the laboratory timescale and is accompanied by an immediate color change from colorless to bright orange. When stored in an atmosphere devoid of excess sulfur dioxide, all these adducts slowly loose SO_2 with regeneration of the corresponding starting materials over a period of several weeks. Neither oxidation of the SO_2 ligand to sulfate nor insertion products have been found, except for complex **6** (vide infra). Changing back to an SO_2-rich environment leads again to quantitative adduct formation. These facts unambiguously demonstrate that the adsorption reaction is an equilibrium process between free and bound SO_2 complexes [Eq. (1)].

$$[PtX(NCN)] + n(SO_2) \rightleftharpoons [PtX(NCN)SO_2)_n] \quad (1)$$

This equilibrium is shifted towards the four-coordinate SO_2-free complexes, if the sulfur dioxide atmosphere is removed. Desorption of SO_2 from the adducts **7**–**10** is accelerated by exposure to air, to solvents free of SO_2, or by reducing the atmospheric pressure, which again quantitatively regenerates complexes **1**–**4**, respectively. Heating can also be used to remove SO_2 from these platinum complexes. An increase in temperature (to 40 °C) leads to the formation of the SO_2-free starting materials within a few minutes. For this latter method

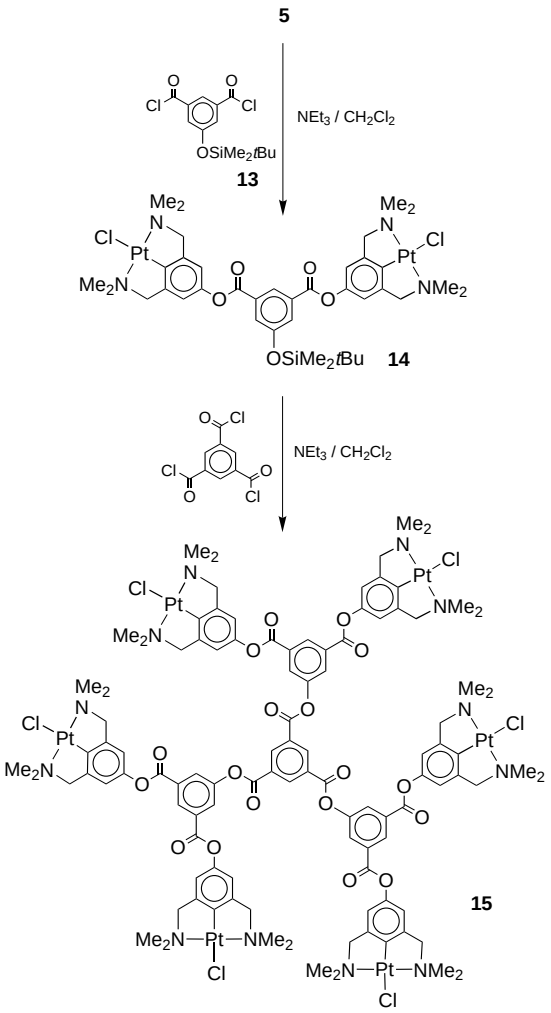

Scheme 2. Synthetic procedure for the convergent preparation of metallodendrimer **15**.

to be effective and quantitative, the Pt complexes must be in solution. In the solid state, thermogravimetric analyses have shown that they do not loose sulfur dioxide at these temperatures. With solid complex **7c**, for example, slow desorption starts at 75 °C, which becomes faster with increasing temperature. At 150 °C, no additional weight is lost; this indicates complete removal of SO_2. This is confirmed by a reduction of the initial mass to 88%, which clearly corresponds to the reversion of **7c** to **1c** (theoretical weight loss: 89%).

Various chemical methods can be used to regenerate the Pt^{II} complexes **1**–**4** from the SO_2 adducts (**7**–**10**). These include the addition of a tertiary amine (e.g., NEt_3), a basic aqueous solution (e.g., 1N NaOH), or a halide source, such as Bu_4NI, to a solution containing the sulfur dioxide adducts.

The SO_2 adduct of the 4-hydroxy platinum complex **5** shows deviating properties with respect to these regeneration methods. Several of the procedures for removing sulfur dioxide developed for the other adducts have been found to be much slower (evaporation in vacuo requires hours rather than minutes to be complete) or ineffective (refluxing a solution of [PtCl(4-OH-Me,Me-NCN)(SO_2)] **11** in THF for several hours did not lead to decolorization and reformation of [PtCl(4-OH-Me,Me-NCN)] **5**).

Finally, adsorption of SO_2 greatly enhances the solubility characteristics of all the platinum complexes studied here. This fact is most prominently demonstrated by the solubility behavior of **5**, which contains a polar organometallic site and a phenolic hydroxy group. As a four-coordinate complex, it is virtually insoluble in most common organic and chlorinated solvents. For example, in benzene, the solubility is lower than 0.2 $g\,L^{-1}$. In SO_2-saturated solution, however, dissolved concentrations of adduct **11** higher than 20 $g\,L^{-1}$ may be obtained. This increased solubility becomes particularly important for macromolecular diagnostic materials that contain several gas-adsorption-active centers. Whereas most of the monomeric complexes are soluble in THF, the tri- and hexa-organoplatinum complexes **3** and **15** fail to dissolve in this solvent and only solubilize as the corresponding sulfur dioxide adducts **9** and **16**, respectively. This is probably due to the change of the coordination geometry of the platinum center from square planar to square pyramidal; this changes the lattice energy of the solid material and reduces the impact of the phenyl factor.[24]

The reactivity of related Pt^{II} complexes such as [PtCl(2-{$CHN(Me)CH_2CH_2NMe_2$}-C_6H_4],[25] (nitrogen donors in *cis* positions) and the ionic complexes [Pt(4-E-Me,Me-NCN)(OH_2)][SO_3CF_3] (with E = H, OH, $OSiMe_2tBu$) with SO_2 were also briefly examined. However, neither NMR nor UV-visible spectroscopy indicate any change comparable with that found for the Pt–SO_2 adsorption products described above. This suggests that no adduct formation takes place. The reason for this lack of reactivity may be the result of a reduced nucleophilicity of these platinum centers relative to that of the neutral sensor sites in complexes **1**–**6** and **15**. It is another indication of the special binding properties of the $[M-X]^+$ entity held in the η^3-*mer* NCN ligand manifold (cf. the role of [Ni–X] unit in the [NiX(NCN)]-catalyzed atom-transfer reaction of CCl_4 with methyl methacrylate).[26]

Spectroscopic properties: The characteristic orange color found for all the SO_2 adducts studied here originates from two Pt→S metal-to-ligand charge-transfer bands that are located in the UV-visible absorbance region. The observed maxima for the adducts **7**–**12** all lie at approximately 350 nm with a broad shoulder (except complexes **10**) at longer wavelength that is primarily dependent on the metal-bound halide (Table 1). The series of SO_2 complexes that contain the unsubstituted NCN ligand (complexes **7a**–**c**) strictly obeys the spectroscopic series upon change of the Pt-bound halide, that is, the absorption maximum shifts towards higher wavelength with increasing electron release of the halide (I > Br > Cl). Surprisingly, this tendency is not seen in the series of complexes that contain the siloxy group (i.e., $OSiMe_2tBu$) as the substituent in the position *para* to the metal-bound carbon atom (**8a**–**c**). The bromide complex **8b** has a remarkably high energy gap for the corresponding electronic transition with a maximum at 333 nm, whereas the maxima of **8a** (X = Cl) and **8c** (X = I) were found at 350 nm and 368 nm, respectively. A similar halide dependence is found in the series of complexes free of SO_2 (**2a**–**c**); in contrast to the chloride and iodide species, the absorption spectrum of the bromide complex **2b** differs considerably from its unsubstituted analogue **1b**.

0947-6539/00/0608-1434 $ 17.50+.50/0 *Chem. Eur. J.* **2000**, *6*, No. 8

Table 1. UV-visible[a] and relevant IR[b] spectroscopic data for complexes **1**–**12**.

	Complex	UV-visible λ_{max} [nm] (ε)	IR $\tilde{\nu}$ [cm^{-1}] $\tilde{\nu}_s(SO_2)$	$\tilde{\nu}_{as}(SO_2)$	Ref.
[PtX(4-E-R,R′-NCN)]					
1a	R = R′ = Me, E = H, X = Cl	279 (9.7)			[18b]
1b	R = R′ = Me, E = H, X = Br	281 (9.8)			[18b]
1c	R = R′ = Me, E = H, X = I	285 (12.8)			[18b]
2a	R = R′ = Me, E = OSiMe$_2$*t*Bu, X = Cl	278 (14.2)			[22]
2b	R = R′ = Me, E = OSiMe$_2$*t*Bu, X = Br	259 (16.5)			
2c	R = R′ = Me, E = OSiMe$_2$*t*Bu, X = I	283 (16.5)			
3	[C$_6$H$_3$-{C(O)-O-NCN-PtCl}$_3$]	276 (26.5)			[22]
4a	R = R′ = Et, E = H, X = I	277 (12.2)			
4b	R = Me, R′ = Et, E = H, X = Cl	277 (7.2)			
5	R = R′ = Me, E = OH, X = Cl[c]	277 (10.9)			
6	R = R′ = Me, E = H, X = 4-tolyl	338 (1.0)			
[PtX(4-E-R,R′-NCN)(SO$_2$)]					
7a	R = R′ = Me, E = H, X = Cl	352 (6.5), 408 (1.7)	1076	1238	
7b	R = R′ = Me, E = H, X = Br	356 (6.9), 410 (1.9)	1076	1230	
7c	R = R′ = Me, E = H, X = I	364 (6.8), 410 (1.4)	1076	1226	
8a	R = R′ = Me, E = OSiMe$_2$*t*Bu, X = Cl	350 (7.8), 421 (2.3)	1074	1226	
8b	R = R′ = Me, E = OSiMe$_2$*t*Bu, X = Br	333 (9.3), 395 (2.4)	1074	1215	
8c	R = R′ = Me, E = OSiMe$_2$*t*Bu, X = I	368 (9.4), 422 (2.2)	1074	1215	
9	[C$_6$H$_3$-{C(O)-O-NCN-PtCl}$_3$(SO$_2$)$_3$]	351 (14.8), 402 (4.3)	1075 (sh)	1226	
10a	R = R′ = Et, E = H, X = I	368 (sh; 1.5)	1067 (sh)	1219	
10b	R = Me, R′ = Et, E = H, X = Cl	353 (6.3), 401 (1.5)	1078	1234	
11	R = R′ = Me, E = OH, X = Cl[d]	350 (8.7), 419 (2.0)	1072	1236	
12	R = R′ = Me, E = H, X = 4-tolyl	357 (4.1), 410 (1.3)	1063	1215	

[a] From CH_2Cl_2 solution, ε [10^3 M^{-1}cm^{-1}]. [b] In $CHCl_3$. [c] ν(O–H) 3304 cm^{-1}; [d] ν(O–H) 3306 cm^{-1}.

Time-resolved UV-visible spectroscopic measurements (stopped flow; benzene solution) indicate that the reaction of arylplatinum complexes with SO_2 is complete within 50 μs. Decreasing the mixing temperature from ambient temperature to 7 °C did not significantly slow down the process and, hence, no definite mechanistic conclusions on the adsorption reaction (pre-equilibria, site of initial attack) can be drawn from these measurements.

Infrared spectroscopic investigations have concentrated on the assignment of the symmetric and asymmetric stretching vibrations of the bound SO_2 molecule (Table 1). In all the adducts the signals assigned to these vibrations were found between 1238 and 1214 cm^{-1} (ν_s) and 1080 and 1064 cm^{-1} (ν_{as}) (measured in $CHCl_3$ saturated with SO_2). These regions are characteristic for sulfur dioxide bound to d^8 metal centers.[7b] However, complexes **10a** and **10b**, which contain ethyl substituents on the metal-bound amines, do not clearly exhibit an absorbance at lower wavenumber, probably because of the overlap with the very strong ν_{as} band from free sulfur dioxide.[7c] Furthermore, the values obtained for complexes **7a**–**c** in this study corroborate well with the frequencies found earlier from Nujol measurements of the solid materials.[10]

The NMR characteristics of the square-planar complexes **1**–**6** have been discussed earlier.[10, 14] For the SO_2 adducts **7**–**12**, comparison of the NMR resonance data with those of the corresponding starting materials **1**–**6** is illustrative. The ^{1}H NMR spectra of the SO_2 adducts **7**–**9**, **11**, and **12**, reveal a characteristic down-field shift of the resonance signals of the NCH_3 and CH_2N protons ($\Delta\delta = 0.14$ and 0.23 ppm, respectively, in SO_2 saturated solutions of $CDCl_3$, with $\Delta\delta = \delta_{(adduct)} - \delta_{(free\ complex)}$, Table 2) when compared with the corresponding SO_2 free complexes.[27] The same chemical shifts of the two benzylic CH_2N protons and of both the nitrogen-bound methyl groups of the (NCN) ligand moiety in **7** have been demonstrated.[10] In an environment which is subsaturated with sulfur dioxide, one single set of signals is observed which is positioned between that found for the SO_2-free complex and the adduct.[28] Similar conclusions can be drawn from the analyses of the $^{13}C\{^1H\}$ NMR spectroscopic data (Table 3); adduct formation is pronounced by a notable shift of the nitrogen-bound methyl carbons towards higher field, which indicates an enhanced shielding of these nuclei. The position of the relevant signals in the ^{1}H or $^{13}C\{^1H\}$ NMR spectrum is directly dependent on the total concentration of sulfur dioxide and can therefore be used to indicate and quantify the presence of dissolved SO_2 (Figure 2). Remarkably, the trifurcate organoplatinum complex **9** shows one set of signals only, regardless of the concentration of SO_2. This unambiguously indicates that all three Pt^{II} centers are equally coordinating to SO_2.

A particular NMR behavior has been found for the platinum compounds **4a** and **4b** with prochiral CH_2 groupings at the nitrogen-bound carbons because of the presence of ethyl- instead of methyl-amino substituents.[29] In the case of the diethylamino compound **4a**, the multiplets that result from the NC*H*$_2$Me protons at $\delta = 3.69$ and 2.92 (ABX_3 pattern) undergo a shift of 0.06 ppm (high field) and 0.01 ppm (down field), respectively, upon addition of SO_2. Also the benzylic protons do not show a characteristic change as observed for the adducts **7**–**9** and, hence, the resonance signals of **10a** appear at virtually the same position as found for SO_2-free **4a**. This indicates that coordination of SO_2 to **4a** is, if it occurrs at all, very weak. A different situation accounts for **10b** and **4b**; from the benzylic protons, which are split into two sets of AB doublets (assigned to the *rac* and *meso* isomers,

Table 2. ^{1}H NMR data for complexes **1**–**12**.[a]

	Complex	C_{aryl}-H	$ArCH_2N$ (^3J(H,Pt))	NCH_3 (^3J(H,Pt))	Other H	Ref.
[PtX(4-E-R,R′-NCN)]						
1a	R = R′ = Me, E = H, X = Cl	6.99 (t), 6.80 (d)	4.02 (46)	3.07 (38)		
1b	R = R′ = Me, E = H, X = Br	7.03 (t), 6.80 (d)	4.02 (46)	3.11 (38)		
1c	R = R′ = Me, E = H, X = I	7.03 (t), 6.83 (d)	4.03 (46)	3.18 (39)		
2a	R = R′ = Me, E = OSiMe$_2$*t*Bu, X = Cl	6.35	3.96 (46)	3.07 (38)	0.96, 0.16	[22]
2b	R = R′ = Me, E = OSiMe$_2$*t*Bu, X = Br	6.33	3.96 (45)	3.11 (38)	0.96, 0.16	
2c	R = R′ = Me, E = OSiMe$_2$*t*Bu, X = I	6.73	3.96 (45)	3.16 (39)	0.96, 0.16	
3	[C_6H_3-{C(O)-O-NCN-PtCl}$_3$]	6.73	4.05 (41)	3.11 (36)	9.15	[22]
4a	R = R′ = Et, E = H, X = I	6.97 (t), 6.70 (d)	4.06 (37)	3.69,[b,c] 2.92 (22)[c]	1.52	[29a]
4b	R = Me, R′ = Et, E = H, X = Cl					
	major isomer	6.96 (t), 6.78 (d)	4.24 (29), 3.81 (56)	3.13 (39), 3.33 – 2.80 (m)[b,c]	1.47	
	minor isomer	6.96 (t), 6.78 (d)	4.21 (38), 3.83 (53)	3.11 (39), 3.33 – 2.80 (m)[b,c]	1.50	
5	R = R′ = Me, E = OH, X = Cl	6.39	3.98 (45)	3.07 (30)		
6	R = R′ = Me, E = H, X = 4-tolyl	6.9	4.16 (43)	2.95 (43)	7.64, 7.02, 2.33	[18b]
[PtX(4-E-R,R′-NCN)(SO$_2$)]						
7a	R = R′ = Me, E = H, X = Cl	7.08 (t), 6.88 (d)	4.25 (41)	3.22 (32)		
7b	R = R′ = Me, E = H, X = Br	7.08 (t), 6.88 (d)	4.25 (41)	3.26 (33)		
7c	R = R′ = Me, E = H, X = I	7.11 (t), 6.87 (d)	4.25 (42)	3.33 (36)		
8a	R = R′ = Me, E = OSiMe$_2$*t*Bu, X = Cl	6.43	4.19 (41)	3.22 (32)	0.98, 0.18	
8b	R = R′ = Me, E = OSiMe$_2$*t*Bu, X = Br	6.42	4.18 (42)	3.25 (33)	0.97, 0.18	
8c	R = R′ = Me, E = OSiMe$_2$*t*Bu, X = I	6.41	4.20 (41)	3.32 (35)	0.97, 0.18	
9	C_6H_3-(C(O)-O-NCN-PtCl)$_3$(SO$_2$)$_3$	6.84	4.27 (41)	3.24 (31)	9.13	
10a	R = R′ = Et, E = H, X = I	6.96 (t), 6.69 (d)	4.06 (37)	3.63,[b,c] 2.93 (21)[c]	1.50	
10b	R = Me, R′ = Et, E = H, X = Cl					
	major isomer	6.99 (t), 6.79 (d)	4.24 (17), 4.01 (25)	3.14 (36), 3.48,[b,c] 3.15[b,c]	1.33	
	minor isomer	6.98 (t), 6.79 (d)	4.17,[b] 4.06 (18)	3.13 (36), 3.34,[b,c] 3.08[b,c]	1.38	
11	R = R′ = Me, E = OH, X = Cl	6.44	4.21 (41)	3.22 (31)		
12	R = R′ = Me, E = H, X = 4-tolyl	7.05 (t), 6.89 (d)	4.41 (37)	3.34 (36)	7.70, 7.12, 2.38	

[a] Singlet signals from $CDCl_3$ solutions unless stated otherwise; doublet (d), triplett (t), multiplett (m); δ (J [Hz]). [b] ^3J(Pt,H) not resolved/observed. [c] NCH_2Me; ABX_3 pattern of NCH_AH_BMe; ^2J(H,H) = 12.3 Hz, ^3J(H,H) = 7.2 Hz.

Table 3. ^{13}C NMR data for complexes **1**–**12**.[a]

	Complex	C_{ipso}	C_{ortho}	C_{meta}	C_{para}	$ArCH_2N$	R, R′	Other C	Ref.
[PtX(4-E-R,R′-NCN)]									
1a	R = R′ = Me, E = H, X = Cl	144.5	142.7	122.6	118.6	77.1	53.7		[18b]
1b	R = R′ = Me, E = H, X = Br	145.7	142.7	122.8	118.7	76.8	54.5		[18b]
1c	R = R′ = Me, E = H, X = I	149.6	143.4	123.4	119.2	76.9	56.3		
2a	R = R′ = Me, E = OSiMe$_2$*t*Bu, X = Cl	152.6	143.8	136.2	111.4	77.7	54.5	25.7, 18.1, – 4.4	[22]
2b	R = R′ = Me, E = OSiMe$_2$*t*Bu, X = Br	152.6	143.7	137.5	111.3	77.4	55.0	25.6, 18.0, – 4.5	
2c	R = R′ = Me, E = OSiMe$_2$*t*Bu, X = I	152.6	144.0	141.1	111.3	76.9	56.4	25.5, 18.0, – 4.5	
3	C_6H_3-(C(O)-O-NCN-PtCl)$_3$	147.3	144.1	143.1	112.8	77.6	54.5	163.7, 135.8, 131.3	[22]
4a	R = R′ = Et, E = H, X = I	146.2	145.4	122.8	117.4	69.0	61.7[c]	13.5	[29a]
4b	R = Me, R′ = Et, E = H, X = Cl								
	major isomer	144.1	143.9	122.8	118.6	73.3	59.4,[c] 53.7	12.9	
	minor isomer	144.2	143.8	122.8	118.7	73.8	59.7,[c] 53.5	13.0	
5	R = R′ = Me, E = OH, X = Cl [b]	154.3	143.4	133.1	106.7	77.3	54.0		[20]
6	R = R′ = Me, E = H, X = 4-tolyl	172.0	145.1	122.4	118.1	81.1	54.9	179.2, 138.9, 129.6, 127.4, 21.0	[18b]
[PtX(4-E-R,R′-NCN)(SO$_2$)]									
7a	R = R′ = Me, E = H, X = Cl	147.4	142.4	125.4	120.5	75.9	53.8		
7b	R = R′ = Me, E = H, X = Br	150.1	142.5	125.6	120.6	75.6	54.4		
7c	R = R′ = Me, E = H, X = I	151.9	142.7	125.5	120.4	75.1	55.4		
8a	R = R′ = Me, E = OSiMe$_2$*t*Bu, X = Cl	154.3	142.9	138.7	112.6	75.7	53.5	25.5, 18.0, – 4.5	
8b	R = R′ = Me, E = OSiMe$_2$*t*Bu, X = Br	154.3	142.9	140.3	112.5	75.5	54.3	25.5, 18.0, – 4.5	
8c	R = R′ = Me, E = OSiMe$_2$*t*Bu, X = I	154.3	143.4	141.4	112.4	75.2	55.5	25.6, 18.1, – 4.5	
9	[C_6H_3-{C(O)-O-NCN-PtCl}$_3$(SO$_2$)$_3$]	148.7	144.7	143.4	114.0	75.9	54.0	163.4, 135.9, 131.2	
10a	R = R′ = Et, E = H, X = I	146.3	145.0	123.0	117.6	68.0	61.7[c]	13.4	
10b	R = Me, R′ = Et, E = H, X = Cl								
	major isomer	145.4	143.5	124.2	119.3	72.4	59.5,[c] 51.7	12.0	
	minor isomer	145.5	143.4	124.1	119.2	72.8	59.9,[c] 51.8	12.5	
11	R = R′ = Me, E = OH, X = Cl	154.7	143.0	138.0	108.3	75.7	53.9		
12	R = R′ = Me, E = H, X = 4-tolyl	[d]	142.8	124.9	120.5	75.4	55.0	[d] 138.3, 129.0 126.2, 22.0	

[a] $CDCl_3$ solutions unless stated otherwise. [b] In $CDCl_3$/[D_6]DMSO. [c] NCH_2Me. [d] C_{ipso} not observed.

0947-6539/00/0608-1436 $ 17.50+.50/0 *Chem. Eur. J.* **2000**, *6*, No. 8

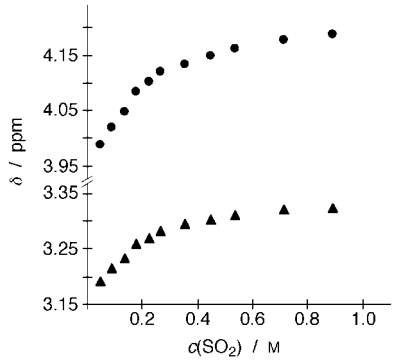

Figure 2. Diagnostic characteristics of the ligand resonance signals in ^{1}H NMR spectroscopy. The chemical-shift dependence on the concentration of SO_2 is shown for the benzylic (top, circles) and methyl (bottom, triangles) protons of a mixture of **2c** and **8c**.

respectively), the resonances at lower frequency are shifted characteristically upon addition of SO_2, whereas the signals around $\delta = 4.2$ are unaffected. A similar behavior is found for the NCH_2Me protons. Additional evidence for sulfur dioxide bonding and a concomitant change of the geometry around the metal center in **10b** is gained from consideration of the coupling constants, which decrease substantially when SO_2 is present in solution. These results indicate that in contrast to **4a** (which contains two NEt_2 groupings), coordination of SO_2 to **4b** (which bears two NEtMe groupings) occurs for both isomers. Apparently, one methyl group on the nitrogen donor already gives space enough for coordination, while two larger substituents (e.g., NEt_2) prevent bonding to SO_2, unless their steric impact is reduced (as, for example, in $N(CH_2)_4$).[9e] This effect is best understood by considering the puckering of the two five-membered metallacycles Pt-N-C-C-C_{ipso} with the aryl plane of the NCN ligand in the square-planar PtX(NCN) complexes (C_S symmetry).[14, 29a] Owing to this puckering, the two alkyl substituents on each nitrogen are positioned pseudo-axially and pseudo-equatorially, and the two axial substituents are *anti*-planar to each other (see Newman projection in Scheme 3). Coordination of SO_2 forces one metallacycle to invert this relative axial-equatorial orientation of the substituents (C_v symmetry). Such a structure is minimized when only little repulsion of the two syn-planar, co-axially positioned substituents occurs, that is, when at least one of these substituents is a CH_3 group.[14] In the case of **4a**, no such configuration is possible and, as a consequence of the steric repulsion of the mutually co-axial ethyl groups, the nitrogen atom is continuously forced to adopt a coplanar

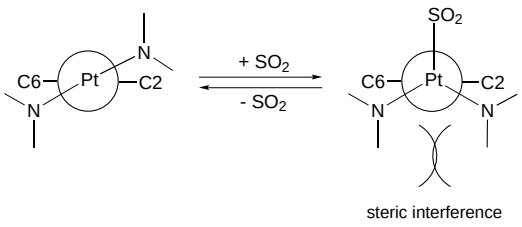

Scheme 3. Newman projection along the Pt–C_{ipso} axis, illustrated at the equilibrium of *meso*-**4b** and *meso*-**10b**; because of the repulsion of the axial substituents on nitrogen in the adduct (syn-orientation), only the product is formed that contains the bulky substituents in equatorial positions.

position with respect to the aryl ring. Hence, the puckering diminishes and strong coordination of SO_2 is hampered. This conclusion is corroborated by the observation that crystallization from SO_2-saturated solutions afforded **4a** instead of **10a** (vide infra). In **4b**, however, axial orientation of the methyl groups is possible in both the *rac* and the *meso* isomers. In the latter case, two diastereotopic adducts may form in princple, namely those with either axial or equatorial methyl groups. However, only one adduct, *meso*-**10b**, is observed spectroscopically (along with *rac*-**10b**), which contains the methyl groupings in pseudo-axial and the ethyl substituents in equatorial orientation (see ^{13}C NMR data, Table 3). Such a site-selective bonding of SO_2 is expected to occur, when steric repulsion of large substituents in co-axial positions is dominant.

When sulfur dioxide is added to the tolyl-complex [Pt(4-C_6H_4Me)(NCN-Me,Me)] **6**, a set of signals appears, which points to the formation of a SO_2 adduct **12**. Besides **12**, another compound is formed gradually that is characterized by two new AB doublets in the aromatic region ($\delta = 7.93$ and 7.25) of the ^{1}H NMR spectrum, together with shifted signals assigned to the protons of the NCN ligand. In contrast to the AB patterns for **6** and **12**, these new signals, which are due to the *para*-tolyl ligand, do not contain characteristic ^{195}Pt–^{1}H couplings. This suggests the formation of a product that results from the irreversible insertion of SO_2 into the metal-carbon bond.[30] No attempts have been made to isolate and further identify this product.

Based on these NMR investigations, it becomes evident that for all [PtX(NCN)] complexes with X = Cl, Br, and I, adduct formation with SO_2 occurs, provided that the ligating nitrogen atoms contain at least one methyl substituent. Ethyl substituents are already bulky enough to prevent significant coordination of SO_2 to the metal center. Moreover, complexes with X = *p*-tolyl form adducts that bind SO_2 as strong as the corresponding halide complexes, since the chemical shift differences of the diagnostic protons are in a similar range. This implies that steric repulsion of the tolyl ligand with respect to the SO_2 molecule is negligible and the oxygen atoms of SO_2 are probably directed towards the NCN-aryl π-system.

Solid-state studies: In order to unambiguously establish the nature of **11** and the SO_2 complex of **4a**, crystal structure determinations were carried out for complex **11** and attempted for **10a**. Generally, crystals were grown by slow diffusion of pentane into a SO_2-saturated CH_2Cl_2 solution of the arylplatinum species; this afforded orange needles of **11** and colorless blocks of **4a** suitable for X-ray analysis. For comparison, the structures of **8c**[12] and **7b**[10] will also be discussed.

The molecular structure of **8c** is shown in Figure 3a (for selected bond lengths and angles, see Table 4). The sulfur dioxide molecule is coordinated through S in a η^1-bonding mode to the platinum center. Platinum is in a pseudo-square-pyramidal environment with SO_2 in the apical position. The angles to the four basal atoms are between 91.4(2)° and 98.1(1)°. No disorder in the position of SO_2 has been detected that could rise from partial coordination to iodide. This selective bonding to Pt is remarkable with respect to the

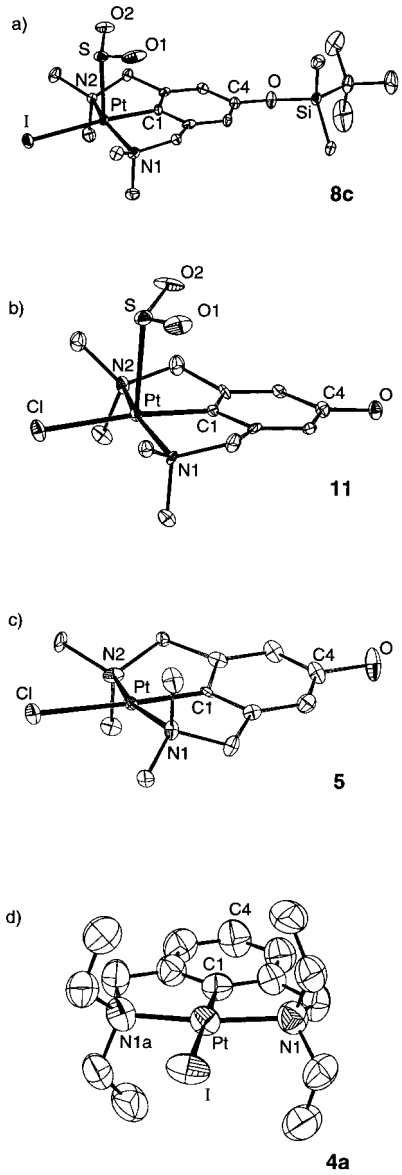

Figure 3. Perspective diagrams (50 % probability) and numbering schemes of the structures of the adducts a) **8c** [PtI(4-OSiMe$_2$*t*Bu-Me,Me-NCN)(SO$_2$)] and b) **11** [PtCl(4-OH-Me,Me-NCN)(SO$_2$)] and of the SO$_2$-free complexes c) **5** [PtCl(4-OH-Me,Me-NCN)] and d) **4a** [PtI(Et,Et-NCN)]. Hydrogen atoms and the second independent molecule in the unit cell of **4a** are omitted for clarity.

expected competitive behavior of iodide in nucleophilicity and size.[31] Related structures of organometallic Pt^{II}-iodide complexes are known that contain the SO$_2$ molecule coordinated to iodide such as in [Pt(Me)(I-SO$_2$)L$_2$] (L = PPh$_3$).[32] Nevertheless, the predictions of the geometry for complexes of the type [ML{SO$_2$}][8] derived from extended Hückel calculations are clearly demonstrated.[7a] These include i) selective η^1 coordination of sulfur dioxide (note that both S–O bonds are statistically equal in length within experimental error), ii) a pyramidal geometry of the SO$_2$ plane with respect to the Pt–S axis (θ of the plane defined by SO$_2$ with the Pt–S axis is approximately 116°), and iii) bending of the oxygen atoms away from iodide (π donor) and towards the aryl unit of the NCN ligand (π acceptor). This last point is evident in the structure of **8c**, whereas in the bromide complex **7b** the orientation of the sulfur dioxide ligand is less predictable (the vector of one S–O bond being nearly collinear with that of the Pt–Br bond). This may rise from a more prominent π-donor–acceptor relationship in complex **8c**, induced by the halide and the oxo substituent on the aryl ligand. Probably this is also the reason for the shorter metal-to-sulfur bond length in **8c** (2.479(2) Å) relative to this bond in **7b** (2.613(7) Å). An energy profile of the rotation of the SO$_2$ ligand around the Pt–S bond axis (analysis of the steric factors by CAChe techniques[33]) does not exceed a maximal difference of 6.0 kJ mol^{-1}. This emphasizes the importance of electronic arguments and crystal-packing effects in the orientation of the sulfur dioxide molecule in the apical position, as demonstrated by the crystal structures of **8c** and **7b**.

Table 4. Selected bond lengths [Å] and angles [°] for **4a** and **5**,[a] and the SO$_2$ complexes **8c**[b] and **11**.

	4a (X = I) molecule 1	**4a** (X = I) molecule 2	**8c** X = I	**5** X = Cl	**11** X = Cl
bond lengths					
Pt–C1	1.929(7)	1.928(6)	1.946(6)	1.915(9)	1.923(10)
Pt–X	2.7328(6)	2.7300(6)	2.718(1)	2.434(2)	2.423(3)
Pt–N1	2.089(5)	2.095(5)	2.112(4)	2.094(8)	2.106(8)
Pt–N2	2.089(5)	2.103(4)	2.113(5)	2.082(8)	2.096(8)
Pt–S	–	–	2.479(2)	–	2.531(3)
S–O1	–	–	1.443(4)	–	1.444(9)
S–O2	–	–	1.433(6)	–	1.430(9)
bond angles					
N1-Pt-N2	165.37(17)	164.7(2)	156.7(2)	163.9(3)	160.5(3)
C1-Pt-X	180.00(8)	178.15(13)	174.4(2)	177.4(4)	173.1(3)
C1-Pt-N1	82.68(12)	82.1(2)	81.2(2)	81.6(4)	82.3(4)
C1-Pt-N2	82.68(12)	82.6(2)	81.5(2)	82.4(4)	81.5(4)
X-Pt-N1	97.32(12)	98.54(16)	98.15(13)	97.9(2)	97.2(2)
X-Pt-N2	97.32(12)	96.70(12)	97.58(15)	98.2(2)	97.7(2)
X-Pt-S	–	–	94.14(4)	–	96.90(11)
C1-Pt-S	–	–	91.44(18)	–	90.0(3)
N1-Pt-S	–	–	98.1(1)	–	93.2(3)
N2-Pt-S	–	–	97.8(2)	–	97.6(2)
O1-S-Pt	–	–	103.3(2)	–	105.6(4)
O2-S-Pt	–	–	105.9(2)	–	103.6(4)
O1-S-O2	–	–	113.6(3)	–	113.4(6)
C4-O-E	–	–	132.5(4) (E = Si)	113(9) (E = H)	109.5 (E = H)

[a] From ref. [20]. [b] From ref. [12].

The molecular structure of the adduct [PtCl(4-OH-Me,Me-NCN)(SO$_2$)] **11** displays similar features as described for the 4-OSiMe$_2$*t*Bu complex **8c** (Figure 3b; selected bond lengths and angles in Table 4). Compared with its SO$_2$-free 4-OH analogue **5** (Figure 3c),[20] only slight differences in bond lengths and angles are found. Remarkably, even the hydrogen-bond motif,[34] which interconnects the single molecules to linear chains through strong Pt–Cl···H–O bonds, is conserved in the sulfur dioxide adduct **11** (see Table 5). An

Table 5. Hydrogen-bond characteristics for compound **5** and the corresponding SO$_2$ complex **11**.

	O–H	H···Cl	O···Cl	O–H···Cl
5[a]	0.84(13)	2.32(13)	3.127(8)	161(15)
11[b]	0.84	2.31	3.126(8)	163.9

[a] The hydrogen atom was located on the difference Fourier map and further refined (from ref. [20]). [b] Located on the difference Fourier map and refined with a rotating model.

0947-6539/00/0608-1438 $ 17.50+.50/0 *Chem. Eur. J.* **2000**, *6*, No. 8

intriguing feature of the crystal structure of **11** is the considerably short distance between the sulfur nucleus and the metal-bound chloride of a neighboring molecule (3.253(4) Å).[35] This gives rise to a β-type network with Pt···S···Cl interactions that are perpendicular to the (former) α-type network induced by Pt–Cl···H–O hydrogen bonding. The result is a two-dimensional supramolecular assembly as depicted in Figure 4, due to molecular recognition

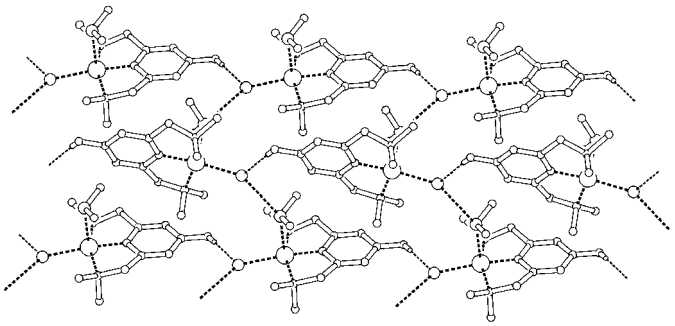

Figure 4. The crystal structure of **11** [PtCl(4-OH-Me,Me-NCN)(SO_2)]. The view along the *y* axis shows the supramolecular self-assembly of **11** in the solid state by directional Pt–Cl···H–O hydrogen bonding and superimposed Pt···S···Cl interactions, which results in the formation of a β-type network.

(hydrogen-bonded network) and substrate-mediated (SO_2) interlocking of these chains. Materials such as **11** are particularly attractive for crystal engineering, since they combine the directional properties of the α-type interaction and the self-organization through reversibly formed β-type interactions.

Attempts to crystallize **10b** failed. In all cases, crystals of **4a** were obtained exclusively. However, the structural details of the molecular geometry of **4a** in the solid state gives valuable information concerning the weak tendency of **4a** to form SO_2 complexes. Two inequivalent molecules of **4a** were found in the crystal lattice; one is C_{2v} symmetric (**4a-*C*$_2$**) and the second is asymmetric (**4a-*C*$_1$**). The molecular structure (Figure 3d) is characterized by a platinum(II) metal center in a slightly distorted square-planar geometry, bound to the η^3-*mer*-coordinating NCN ligand and an iodide ion. Bond lengths and angles (Table 4) are closely related to the values found for similar complexes.[9e, 18b, 36] The puckering of the five-membered metallacycles with the plane of the aryl ring, characterized by the torsion angle of N1-Pt-C1-C2, does not exceed 4.3(3)°. This is significantly smaller than the values found typically in the corresponding NMe_2 complexes (around 10°). This increased coplanarity of the aryl plane and the square plane around the platinum center probably originates from steric repulsion of the four ethyl substituents and results in a flattening of the five-membered chelate rings, that is, in a less pronounced axial/equatorial orientation of these ethyl groups. Consequently, replacment of both nitrogen-bound methyl by ethyl groups gives rise to an increased hindrance of the potential coordination sites at the platinum center.[9e] Note that the NMR studies already indicated that **4a** did not show any notable interaction with SO_2 in solution (vide supra).

Thermodynamics: To get further information concerning the nature and the stability of the Pt–SO_2 binding in the complexes **7**–**11** in solution, UV-visible spectrophotometric measurements at varying concentrations of SO_2 were carried out (Figure 5). The overlapping spectra do not show an isosbestic point, probably because of the coinciding strong absorbance of free SO_2 (relevant below 320 nm), which entirely covers the absorption bands of the SO_2-free complexes **1**–**5**. Increasing the concentration of sulfur dioxide leads to a higher absorbance at λ_{max} (Figure 5).

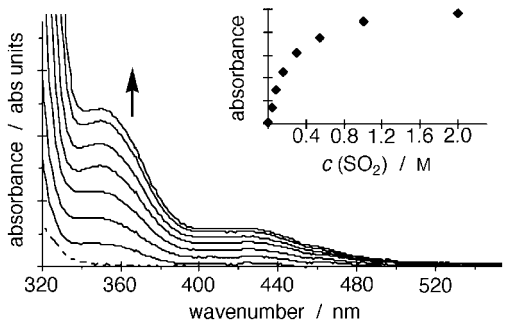

Figure 5. The response of the complex **2a** on changes in the concentration of SO_2, monitored by UV-visible spectroscopy. The spectra correspond to **2a** (dashed line) and to mixtures of **2a** and **8a** at 40, 80, 160, 300, 540, 1000 mM, and saturated solutions of SO_2. Inset: Variation of the extinction at 350 nm.

Equilibrium constants K_f of the equilibrium between the SO_2 adducts **7**–**11** and their four-coordinate starting materials were determined by titration of solutions of complexes **1**–**5**, respectively, with SO_2 (dissolved in benzene). The constants K_f were evaluated by recording A_c (absorbance λ_{max} of the adduct at a SO_2 concentration *c*, relative to A_∞, the absorbance in SO_2-saturated benzene solution) versus the concentration of sulfur dioxide. These plots are shown in Figure 6 for the reactions of sulfur dioxide with [PtI(4-OSiMe$_2$*t*Bu-Me,Me-NCN)] **2c** (as representative for

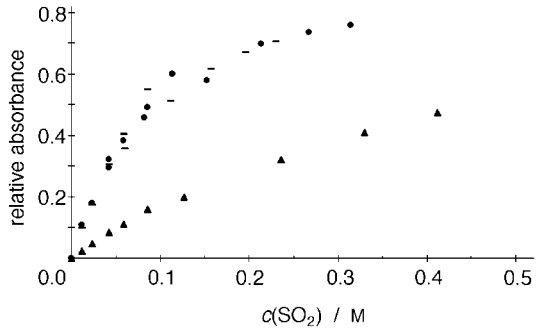

Figure 6. Titration curves for various mono- (**2c**, circles; **4b**, triangles) and multimetallic sensor materials (**3**, bars) against SO_2.

the monometallic NMe_2 complexes **1**, **2**, and **5**), the dendritic Pt_3 species **3**, and [PtI(4-H-Et,Me-NCN)] **4b**. The molarity in SO_2 was adjusted to be always at least ten times higher than the actual concentration of the platinum complexes.[37] This allows us to neglect the change in concentration of SO_2 due to

adduct formation. Hence, from Equation (2), Equation (3) can be deduced and was applied to fit the obtained data points.

$$K_f = \frac{[PtX(NCN)(SO_2)_n]}{[PtX(NCN)][SO_2]^n} \quad (2)$$

$$\frac{[PtX(NCN)(SO_2)_n]_c}{[PtX(NCN)SO_2)_n]_\infty} = \frac{K_f\,[SO_2]^n}{K_f\,[SO_2]^n + 1} \quad (3)$$

The values for the formation constants K_f and the corresponding Gibbs free energies ΔG° are summarized in Table 6. For the reactions starting with monoplatinum species [PtX(4-H-Me,Me-NCN)] **1** or the corresponding 4-substituted complexes **2** or **5**, these data are entirely consistent with the formation of a 1:1 adduct with SO_2 in solution and, hence, are in agreement with the $\Delta\delta$ data obtained by ^{1}H NMR spectroscopy. Despite an earlier hypothesis,[10] no indication for the formation of an octahedral product containing two coordinated molecules of SO_2 has been found. Neither the substituent H or OR on the aryl ligand nor the metal-bound halide seem to affect the equilibrium constant substantially, and, thus, the values found for K_f are all in the same range.

Table 6. Equilibrium constants K_f and ΔG°.[a]

	K_f [M^{-1}]	ΔG° [kJ mol^{-1}]
1a	10.42 (0.42)	− 5.71 (0.10)
1b	9.97 (0.93)	− 5.60 (0.22)
1c	9.80 (1.36)	− 5.56 (0.32)
2a	14.81 (0.35)	− 6.57 (0.06)
2b	8.48 (0.34)	− 5.21 (0.10)
2c	9.51 (1.53)	− 5.49 (0.36)
3	9.90 (1.26)	− 5.59 (0.29)
4b	2.16 (0.09)	− 1.88 (0.10)
5	9.70 (0.63)	− 5.54 (0.15)

[a] Esds in parantheses; for platinum complex **4a**: see text.

The equilibrium between the trimetallic species **3** and **9** is of a different nature and is best described by a 1:3 complex between **3** and SO_2. The similarity of the titration curves of the monometallic and trimetallic sensors suggests that in **3**, the diagnostic platinum centers are virtually independent from each other and behave similar to monomers.[38] This emphasizes the applicability of dendritic materials as useful sensor materials.

Compared with the complexes that contain the pincer ligand with two methyl substituents on the amine donor, for example, complexes **1** or **2**, a significantly lower equilibrium constant has been found for complex **4b**, which contains a bulkier substituent on the amine ligand. The titration measurements still point to a 1:1 adduct with SO_2, whereas in the corresponding NEt_2 complex **4a** a linear relationship between the spectroscopic absorbance and the concentration of SO_2 has been found; this points to a very small equilibrium constant. These observations are remarkable in terms of electronic factors, since the basicity of the nitrogen donor is increased upon changing the substituents in the order Me < Et(< *i*Pr). As a consequence, the nucleophilicity on the metal center and, therefore, its affinity to Lewis acids (e.g., SO_2) is increased. Evidence for the predomination of the steric rather than the electronic arguments in these platinum(II) complexes has arisen from closely related work that includes I_2 as Lewis acid.[39] Data from the X-ray structure determination of platinum complexes with pincer derivatives similar to **4b**, but with N*t*BuMe instead of NEtMe donors, confirmed that the metal center is still accessible by I_2. Adducts that display a square-pyramidal geometry were isolated only when the methyl groups were in pseudo *anti*-conformation with respect to the iodine ligand (pseudo-axial position). A different isomer containing both the *t*Bu groups in the pseudo *anti*-position (methyl groups equatorial) is not stable, probably owing to steric repulsion of the large amine substituents. Hence, the *meso*-conformer of **4b** is supposed to coordinate SO_2 selectively on one site, thus forming a product with axially positioned methyl groups, whereas in *rac*-**4b**, no such site-discrimination is expected. This model is further confirmed by comparison of the spectroscopic data of **10a** and **10b** (vide supra).

Sensor capacity of the square-planar Pt^{II} complexes: The platinum compounds **1**, **2**, **4b**, and **5** and the dendritic Pt_3 complex **3** are all very sensitive towards the presence of low concentrations of sulfur dioxide. Sulfur dioxide coordination is fast (less than 50 μs at room temperature) and can be monitored by various analytical techniques like UV-visible or NMR spectroscopy. No pretreatment of the sensor materials is necessary to activate the platinum complexes. Their selectivity for sulfur dioxide is illustrated by the fact that no evidence for the formation of either adducts with oxygen or with other gases present in the atmosphere (e.g., N_2, CO, CO_2) has been found. Consequently, these platinum-based sensor materials do not need particular protection (e.g., from humidity or air) or pre-activation. None of the frequently observed reactions occur that follow sulfur dioxide coordination on organometallic complexes [e.g., insertion of SO_2 into a metal-carbon (NCN-aryl) bond,[30] oxidation of SO_2 to sulfate in the presence of air or oxygen[40]]. Evident exceptions are complexes that contain unstabilized metal–carbon bonds, like the Pt–C_{tolyl} bond in intermediate complex **12**, in which slow insertion of sulfur dioxide and formation of Pt-S(O)$_2$-C_{tolyl} bonds most probably takes place. A similar insertion into the metal–carbon bond of the Pt(NCN) unit is inhibited, owing to the η^3-*mer-N,C,N* chelation of the NCN ligand that stabilizes the platinum–carbon bond to a large extent.[16]

A variety of facile and non-destructive methods have been elaborated to recycle the sensor materials, including chemical (e.g., competitive sulfur dioxide transfer to halide ions[41] or amines[42]) and physical (e.g., heating, pressure reduction) removal of sulfur dioxide. This broad choice of procedures underlines the suitability of these compounds as sensor devices for repeated and efficient use in various environmental situations.

Even traces of sulfur dioxide gas are sufficient to induce the characteristic color change. By using a solution of **2a** in CH_2Cl_2 (40 μM), it is possible to detect SO_2 concentrations as low as 200 μM by means of UV-visible spectroscopy; this results in a Pt/SO_2 ratio of 1:5. In contrast to these observations, the threshold value for detecting SO_2 has been found to be higher when the sensors are used in the solid state.

0947-6539/00/0608-1440 $ 17.50+.50/0 *Chem. Eur. J.* **2000**, *6*, No. 8

A cellulose surface coated with dendritic macromolecule **3** in a density of 20 nmol mm^{-2} is enough for the detection of an SO_2 concentration of 8.5($\pm$0.5) mg L^{-1}.[12] Interestingly, the threshold values reported here have been determined by routine measurements with common laboratory equipment. This implies that the sensitivity of these sensors must be considerably higher and that threshold limits can be lowered when signal detection is performed on dedicated instruments. Moreover, improvement of the sensor capacity may be achieved by means of signal (light) amplification techniques.[43]

The full reversibility of the SO_2 adsorption is demonstrated by time-resolved photospectroscopic monitoring of a solution of **2c** in dependence of the gaseous environment. Saturation of a solution of **2c** in CH_2Cl_2 (0.1 mM) with SO_2 results in full conversion of the complex into its SO_2 adduct **8c**, which is visualized by maximal absorbance at 368 nm. Continuous addition of air to this solution (slowly) regenerates the four-coordinate starting complex **2c**, which does not absorb at this wavelength. Repetition of this adsorption-desorption cycle by saturating the solution with sulfur dioxide and air, respectively, does not cause a decrease of the observed extinction coefficients, even after several cycles. Figure 7 shows these spectral changes of the detector sites at a fixed wavelength (λ_{max} of the corresponding adduct **8c**, E = OSiMe$_2$*t*Bu, X = I) as a diagnostic response on variation of the atmospheric constitution. These results further provide evidence that there is no loss of SO_2 binding activity, a result which demonstrates the resistance of the Pt-NCN unit towards the applied sensoring conditions. Moreover, the fast response of the detector device to the presence of SO_2 is emphasized by an instantaneous signal transmission.

Another major characteristic of the sensor materials presented here is their activity towards sulfur dioxide both as solid materials or in liquid (in solution or as suspension).

Dendrimer-supported sensor devices: Complete recovery of the diagnostic materials requires a suitable support for the active sites of the sensor. Dendritic supports have an outstanding potential for such purposes, since they combine all advantages of the monomeric complexes with those typically found for heterogeneous or polymeric materials (e.g., easy recovery). Nanofiltration techniques have been successfully used to separate dendritic materials from (reaction) solutions.[44] Most importantly, the presence of well-defined connectivity patterns and exact number of functional (sensor) sites in dendrimers allows *qualitative and quantitative* substrate detection without preceding calibration. This is particularly desirable for solution measurements and contrasts with heterogenous and polymeric sensors, for which the loading of the sensor units must be determined for each batch.

By using this principle,[15] the nanosize dendrimer **15**, which contains six peripheral sensor units, has been tested in the reaction with sulfur dioxide (Scheme 4).[45] When this metallodendrimer **15** is exposed to an atmosphere of SO_2, an instantaneous color change is likewise observed and spectroscopic analyses are consistent with the formation of the hexa-adduct **16**. The shift difference of the characteristic protons in the ^{1}H NMR spectrum ($\Delta\delta$ = 0.12 and 4.20 ppm for the NCH_3 and the benzylic CH_2N protons, respectively) and the extinction coefficient of **16** reveal that all platinum centers in the macromolecule are active on SO_2 binding. Reformation of the SO_2-free material is easily achieved by any of the desorption methods described above. The shape-persistence of the core[46] of these nanosize metallo-dendrimers makes them good candidates for successful recovery from solutions by nanofiltration.

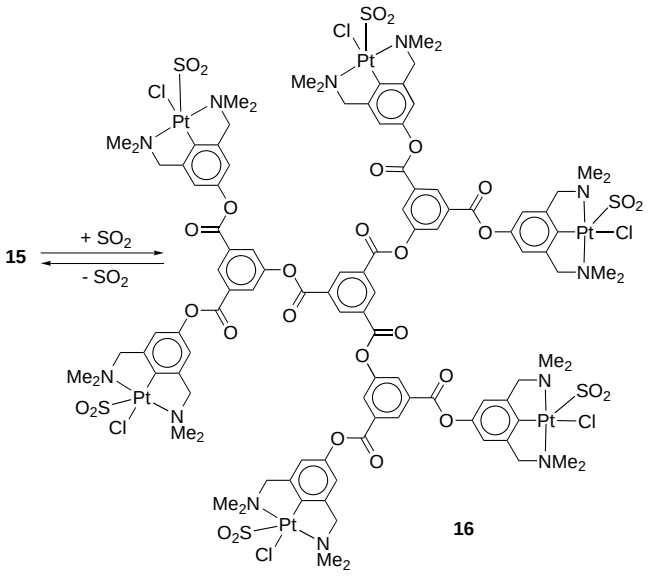

Scheme 4. The activity of multimetallic sensors towards sulfur dioxide adsorption.

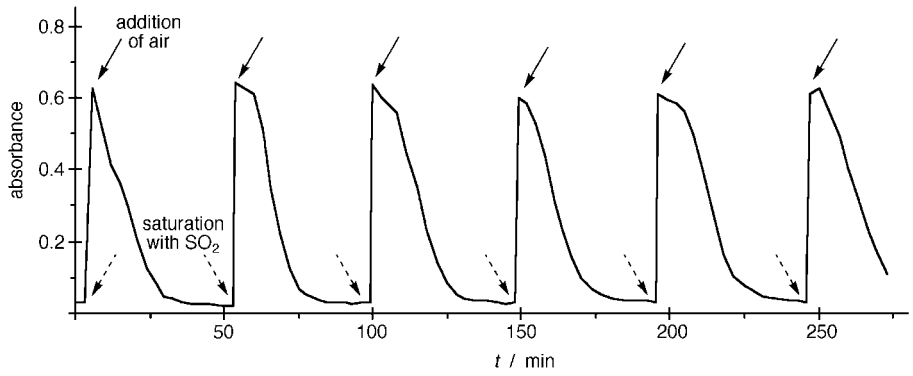

Figure 7. Change of the absorbance of a solution of **2c** at a fixed wavelength (368 nm, λ_{max} of **8c**) as a direct response on the change of the atmosphere. Repetitive cycles do not decrease the activity of the sensor materials.

Conclusion

Multimetallic metallo-dendrimers and monometallic organoplatinum complexes that contain bis-chelating diaminoaryl pincer ligands are efficient sensor materials for the detection of minute levels of sulfur dioxide. Any presence of this gas is

indicated by various analytical techniques, most prominently by a characteristic color change of the initially colorless sensor devices to orange. Adsorption of SO_2 is fully reversible and is fast on the NMR and UV-visible timescale, as the equilibrium of the adsorption reaction is reached within less than 50 μs at temperatures above 5 °C. Further characteristics of these sensor devices comprise facile quantification of the amount of SO_2 present and excellent chemical resistance properties (e.g., towards acids).The diagnostic platinum sites demonstrate outstanding selectivity for SO_2-gas binding. Sensoring of these organometallic bases (the [PtX(NCN)] systems) occurs by a highly specific molecular recognition process of a single acid (SO_2), even in the presence of other (stronger) acids such as HCl, CO_2, or H_2O.

Sensor-active metallo-dendrimers, detector materials which can be recycled easily and quantitatively, are accessible when detection-insensitive sites of the sensor device are coupled to a dendritic framework. Suitable ligand functionalization has been used as the methodology to anchor organoplatinum sites to dendritic cores. This afforded multimetallic sensor materials that are highly efficient and recoverable as exemplified by the metallo-dendrimers **3** and **15**. The well-defined structures of these macromolecules makes them useful for repetitive qualitative and quantitative diagnostic gas sensor applications

Moreover, a new synthon for organometallic crystal engineering has been developed. In the solid state, the SO_2 molecule in complex **11**, which contains a metal-bound chloride, binds to the metal center in a classical bonding mode (i.e., through η^1-Pt–S bond formation) and, in addition, is stabilized by bridging coordination of sulfur to a metal-bound chloride nucleus of a different molecule, hence inducing β-type network formation of **11**. This novel supramolecular synthon has potential application for directing the self-assembly of organometallic building blocks in the solid state.

Experimental Section

General comments: All reactions were performed by using standard Schlenk techniques unless stated otherwise. Sulfur dioxide, $PtCl_2$, SEt_2, Bu_4NF (1 M in THF), HNEtMe, and α,α'-dibromo-*m*-xylene were obtained commercially and used without further purification; 1,3,5-benzenetricarboxylic acid chloride was recrystallized from hot hexane prior to use. Benzene, pentane, and Et_2O were distilled from Na/benzophenone, and CH_2Cl_2 from CaH_2. Elemental analyses were performed by Kolbe, Mikroanalytisches Laboratorium (Mülheim, Germany). ^1H and $^{13}C\{^1H\}$ NMR spectra were recorded on a Bruker AC300 or a Varian Inova 300 spectrometer. All spectra were recorded in $CDCl_3$ solution at 25 °C, unless otherwise stated, and referenced to external TMS ($\delta = 0.00$ ppm, *J* in Hz; see Tables 2 and 3). Spectroscopic studies (UV-visible) were carried out on a Varian Cary 1 spectrophotometer with degassed benzene or CH_2Cl_2 as solvent and standard quartz cuvettes (Table 1). Infrared measurements were performed on a Perkin–Elmer FT-IR spectrometer with CH_2Cl_2 as solvent. Thermogravimetric analyses were carried out in platinum containers (under a continuous flow of nitrogen) on a Perkin–Elmer TGS-2 apparatus using a heating rate of 5 °C min^{-1}. The Pt^{II} complexes **1**,[18b] **2a**,[22] **3**,[22] **4a**,[29a] **5**,[20] and **6**[18b] and the AB_2 branching unit **13**[21] were prepared as described.

[Pt(Cl$_2$)(SEt$_2$)$_2$]: According to a modified literature procedure,[47] SEt_2 (40 mL, 440 mmol) was poured to a suspension of $PtCl_2$ (10.6 g, 39.9 mmol) in benzene (100 mL). Within 0.5 h, all solids had dissolved. The solution was stirred for an additional 0.5 h and subsequently filtered through Celite and evaporated to dryness. The yellow solid was washed with cold pentane (3 × 50 mL) and dried in vacuo for 4 h, to afford 17.6 g of a yellow solid (99 %). Spectroscopic analyses (IR, $^{13}C\{^1H\}$ NMR) indicated a mixture of *trans*- and *cis*-$[PtCl_2(SEt_2)_2]$ and were consistent with literature values.[48]

[PtBr(4-OSiMe$_2$*t*Bu-2,6-{CH$_2$NMe$_2$}$_2$-C$_6$H$_2$] (2b): A modified literature procedure was used.[18b] $AgCF_3SO_3$ (76 mg, 0.30 mmol) was added to a solution of **2a** (165 mg, 0.30 mmol) in acetone (5 mL) and water (0.2 mL). After stirring for 0.5 h under strict exclusion of light, the suspension was filtered through a short pad of Celite. All volatiles were removed in vacuo, and the residue was taken up in water (8 mL). Solid NaBr (87 mg, 0.85 mmol) was added to this suspension and stirring maintained for 0.5 h. The precipitate was collected by filtration, washed with Et_2O (4 mL) and extracted with small portions of CH_2Cl_2 (12 mL total). The combined organic layers were then dried in vacuo, leaving a white solid. Yield: 156 mg (87 %); elemental analysis calcd (%) for $C_{18}H_{33}BrN_2OPtSi$ (596.6): C 36.24, H 5.58, N 4.70; found C 36.39, H 5.51, N 4.78.

[PtI(4-OSiMe$_2$*t*Bu-2,6-{CH$_2$NMe$_2$}$_2$-C$_6$H$_2$] (2c): This compound was prepared in a similar way as described for **2b** by using NaI (141 mg, 0.94 mmol). Yield: 176 mg (91 %); elemental analysis calcd (%) for $C_{18}H_{33}IN_2OPtSi$ (643.6): C 33.59, H 5.17, N 4.35, I 19.72; found C 33.65, H 5.08, N 4.26, I 19.59.

1,3-(CH$_2$NEtMe)$_2$-C$_6$H$_4$: HNEtMe (5.00 g, 83 mmol) was added to α,α'-dibromo-*m*-xylene (5.28 g, 20 mmol) dissolved in Et_2O (30 mL) at 0 °C. The suspension was stirred for 3 h at 0 °C and 12 h at ambient temperature, then poured into NaOH (1M, 100 mL). Extraction with pentane (3 × 100 mL) and subsequent drying of the combined organic fractions over K_2CO_3 yielded, after solvent evaporation in vacuo, a colorless oil, which was purified by bulb-to-bulb distillation. Yield: 3.74 g (84 %); ^1H NMR: $\delta =$ 7.23 (t, ^3J(H,H) = 7 Hz, 1H; Ar*H*), 7.22 (s, 1H; Ar*H*), 7.19 (d, ^3J(H,H) = 7 Hz, 2H; Ar*H*), 3.47 (s, 4H; ArCH_2N), 2.44 (q, ^3J(H,H) = 7.2 Hz, 4H; NCH_2Me), 2.18 (s, 6H; NCH_3), 1.09 (t, ^3J(H,H) = 7.2 Hz, 6H; NCH$_2$CH_3); $^{13}C\{^1H\}$ NMR (75 MHz): $\delta =$ 139.0, 129.8, 128.0, 127,7 (all Ar), 61.9 (Ar*C*H$_2$N), 51.2 (N*C*H$_2$Me), 41.7 (N*C*H$_3$), 12.4 (NCH$_2$*C*H$_3$); MS (70 eV, EI): *m/z* (%): 220 (9) $[M]^+$, 163 (100) $[M - NEtMe]^+$; elemental analysis calcd (%) for $C_{14}H_{24}N_2$ (220.4): C 76.31, H 10.98, N 12.71; found C 76.17, H 11.09, N 12.63.

[PtCl(2,6-{CH$_2$NEtMe}$_2$-C$_6$H$_3$)] (4b): A solution of *n*-BuLi (1.6 mL, 1.66M in hexane, 2.7 mmol) was added dropwise to a solution of 1,3-$(CH_2NEtMe)_2$-C_6H_4 (0.59 g, 2.7 mmol) in pentane (8 mL) at −78 °C. The reaction mixture was allowed to warm to room temperature overnight, and all volatiles were removed in vacuo. The residue was redissolved in Et_2O (10 mL), added to a suspension of $[PtCl_2(SEt_2)_2]$ (1.20 g, 2.7 mmol) in Et_2O (30 mL) and stirred for 16 h. All volatiles were then removed in vacuo, and the residue was washed with pentane (3 × 30 mL) and extracted with CH_2Cl_2 (3 × 30 mL). Concentration of the combined chlorinated fractions to 5 mL followed by the addition of pentane (70 mL) afforded a colorless precipitate, which was isolated by centrifugation and dried in vacuo. Yield: 0.79 g (66 %); elemental analysis calcd (%) for $C_{14}H_{23}N_2ClPt$ (449.9): C 37.38, H 5.15, N 6.23; found C 37.20, H 5.09, N 6.12.

Synthesis of 14 (see Scheme 2): NEt_3 (5 mL, excess) was added dropwise to a suspension of **5** (1.32 g, 3.0 mmol) and **13** (0.50 g, 1.5 mmol) in CH_2Cl_2 (30 mL) over a period of 30 minutes. The reaction mixture slowly became clear and was stirred for additional 24 h before adding H_2O (20 mL). The aqueous phase was separated and extracted with CH_2Cl_2 (2 × 30 mL). The combined organic layers were dried (Na_2SO_4) and evaporated to dryness. The crude product was purified by column chromatography (SiO_2; CH_2Cl_2/acetone 5:1) to afford **14** as an off-white solid (1.05 g, 62 %). ^1H NMR: $\delta =$ 8.53 (t, ^3J(H,H) = 1.4 Hz, 1H; Ar*H*), 7.83 (d, ^3J(H,H) = 1.4 Hz, 2H; Ar*H*), 6.69 (s, 4H; Ar*H*), 4.03 (s, 8H; ^3J(Pt,H) = 38 Hz, ArCH$_2$N), 3.09 (s, 24H; ^3J(Pt,H) broad, not resolved, NCH$_3$), 1.01 (s, 9H; SiCCH$_3$), 0.26 (s, 6H; SiCH$_3$); $^{13}C\{^1H\}$ NMR (75 MHz): $\delta =$ 164.4 (C=O), 156.2 (C–O), 147.5, 144.0, 142.6 (C–Pt), 131.6, 126.2 (C–H), 124.4 (C–H), 112.9(*C*–H) (all Ar*C*), 77.4 (CH$_2$N), 54.4 (NCH$_3$), 25.6 (SiC*C*H$_3$), 18.2 (SiCMe$_3$), −4.4 (SiCH$_3$); FAB-MS: *m/z*: found 1135.24 (calcd 1135.04); elemental analysis calcd (%) for $C_{38}H_{53}Cl_2N_4O_5Pt_2Si$ (1135.0): C 40.21, H 4.79, N 4.94; found C 40.37, H 4.97, N 4.85.

Synthesis of 15 (see Scheme 2): Bu_4NF (0.75 mL, 1M in THF, 0.75 mmol) was added to a solution of **14** (0.85 g, 0.75 mmol) in CH_2Cl_2 (10 mL). After stirring for 30 minutes, 1,3,5-benzenetricarboxylic acid chloride (58 mg, 0.22 mmol) was added and the mixture stirred for 3 days. All volatiles were then removed in vacuo, and the residue washed with THF (2 × 20 mL).

0947-6539/00/0608-1442 $ 17.50+.50/0 *Chem. Eur. J.* **2000**, *6*, No. 8

Then the residual solid was dissolved in CH_2Cl_2 (5 mL) and THF was added (20 mL), which caused precipitation of a fluffy solid after 1 h. The residue was collected and precipitated once more by the same procedure, to afford an off-white solid (0.28 g, 39%). ^{1}H NMR: $\delta = 9.25$ (s, 3H; Ar*H*), 8.82 (br s, 3H; Ar*H*), 8.26 (br s, 6H; Ar*H*), 6.71 (s, 12H; Ar*H*), 4.04 (s, 24H; ^3J(Pt,H) broad, not resolved, $ArCH_2N$), 3.08 (s, 72H; ^3J(Pt,H) broad, not resolved, NCH_3); ^{13}C{^{1}H} NMR (75 MHz): $\delta = 166.5$, 166.4 (both C=O), 159.5, 155.1 (both C–O), 147.5, 143.8, 141.9, 132.3, 113.1, 108.2, 106.5 (all Ar*C*; *C*–Pt not observed), 77.5 (CH_2N), 54.4 (NCH_3); Maldi-TOF: *m/z*: found 3188.1 [*M* – Cl]$^+$; calcd 3185.9.

Preparation of the SO_2 adducts (7–12, 16): Bubbling SO_2 (g) over or through a CH_2Cl_2 solution of the corresponding platinum(II) complex **1–6** or **15** afforded an instantaneous color change from colorless to orange (yellowish, when **4a** is used). The adducts precipitate readily upon addition of pentane or Et_2O. Filtration yielded quantitatively the title compounds **7–12**, and **16** as orange solids (**10a**: yellowish). Drying of any of these SO_2 adducts in vacuo is not possible, because removal of SO_2 immediately takes place, thus regenerating starting complexes **1–6** and **15**, respectively. The spectroscopic characteristics of the adducts **7–12** can be found in Tables 1, 2 and 3. Analytical data for **16**: ^{1}H NMR: $\delta = 9.26$ (s, 3H; Ar*H*), 8.81 (br s, 3H; Ar*H*), 8.32 (br s, 6H; Ar*H*), 6.79 (s, 12H; Ar*H*), 4.24 (s, 24H; ^3J(Pt,H) broad, not resolved, $ArCH_2N$), 3.20 (s, 72H; ^3J(Pt,H) broad, not resolved, NCH_3); UV/Vis (CH_2Cl_2): λ_{max} (ε) = 354 nm (sh, 42000 M^{-1}cm^{-1}), 405 nm (11000 M^{-1}cm^{-1}).

When a SO_2 saturated solution of **10a** or **11** in CH_2Cl_2 was exposed to pentane, crystals were obtained that were suitable for single-crystal X-ray structure determination. The crystals of **10a**, however, were colorless and not orange, as expected from the other sulfur dioxide adducts (**11**: orange needles). Indeed, no SO_2 molecules were found in the unit cell, which contains two independent molecules. The crystals, although grown in the presence of excess sulfur dioxide, contained exclusively compound **4a**.

Recovery of the starting complexes **1–6** or **15** in solution is achieved by i) continuous bubbling of N_2, O_2, or air through a solution of **7–12** or **16**, respectively, in CH_2Cl_2 for 0.5 h (3 h for **11**); ii) heating of a solution to 40 °C for 0.5 h (not suitable for **11**); iii) addition of 30 mol equiv NEt_3 or Bu_4NX (X = Cl, Br, I) to a solution containing the SO_2 adducts; iv) extraction with aqueous NaOH (1M); v) washing the adducts with hexane or Et_2O; vi) evacuation.

Solution measurements: Measurements for the determination of the equilibrium constants K_f were performed by two different methods.

Method A: By UV-visible photospectroscopy: A solution of the appropriate Pt^{II} complex (**1–6**) in degassed benzene (typically 80 *m*M) was titrated with a solution of SO_2 of well-defined concentration (benzene).[37] The absorption spectrum was measured by using standard quartz cuvettes in the wavelength range of 700 to 320 nm at typically ten different concentrations of SO_2. From the absorbance at λ_{max} the concentration of the corresponding SO_2 adduct was calculated (relative to the total concentration of platinum complexes) and compared with the actual concentration of sulfur dioxide. Correlation of the measured curve with an idealized 1:1 adduct of SO_2 and Pt was higher than 0.99 for all recorded equilibria except for **4a**.

Method B: By ^{1}H NMR spectroscopy: Aliquots of gaseous SO_2 (portions of 1 mL, 45 μmol, typically) were added to a well-defined amount of the appropriate Pt^{II} complex (< 0.1 mmol) dissolved in $CDCl_3$ (0.7 mL). The shifts of the resonance signals for the CH_2N and the NCH_3 groups were recorded in relation to those of the SO_2-free complexes and plotted against the actual concentration of SO_2; this resulted in curves that correspond well with the data obtained by method A.

Kinetic measurements were carried out by using routine stopped-flow techniques. The very first UV/Vis spectrum, obtained 0.5 ms after mixing a solution of **1a** with a solution of SO_2 (both in benzene), was identical with the final spectrum of **7a**. The reverse reaction, that is, mixing of a solution of **7a** with **1a** (which has to be ca. 10 times slower, see values of K_f) did not show any kinetic trace and only the final spectrum has been observed.

Structure determination and refinement of 4a and 11: Crystals suitable for X-ray structure analysis were glued onto the tip of a glass fiber, and transferred into the cold nitrogen stream of a Nonius κ-CCD (**4a**) or an Enraf-Nonius CAD4-T diffractometer (**11**). Reduced-cell calculations did not indicate higher lattice symmetry.[49] Crystal data and details on data collection and refinement are collected in Table 7. Data were collected at 293 K (**4a**) or 150 K (**11**), with graphite-monochromated $Mo_{K\alpha}$ radiation ($\lambda = 0.71073$ Å). Absorption corrections (DIFABS/PLATON[50]) were applied for both complexes. The structures were solved by using automated Patterson methods and subsequent difference Fourier techniques (DIRDIF-92[51]). The structures were refined on F^2 using full-matrix least-squares techniques (SHELXL-96[52]); no observance criterion was applied during refinement. Hydrogen atoms were included in the refinement on calculated positions, riding on their carrier atoms, except the oxygen-bound hydrogen in **11**, which was located on the difference Fourier map and subsequently refined with a rotating model. All non-hydrogen atoms were refined with anisotropic thermal parameters. Neutral atomic scattering factors and anomalous dispersion corrections were taken from the *International Tables of Crystallography*. Geometrical calculations and illustrations were performed with PLATON.[50] Crystallographic data (excluding structure factors) for the structures reported in this paper have been deposited with the Cambridge Crystallographic Data Centre as supplementary publication nos. CCDC-133528 (**4a**) and CCDC-133527 (**11**). Copies of the data can be obtained free of charge on application to CCDC, 12 Union Road, Cambridge CB2 1EZ, UK (fax: (+44) 1223-336-033; e-mail: deposit@ccdc.cam.ac.uk).

Table 7. Crystallographic data for complexes **4a** and **11**.

	4a	**11**
color, shape	colorless cube	orange needle
empirical formula	$C_{16}H_{27}IN_2Pt$	$C_{12}H_{19}ClN_2O_3PtS$
formula weight	569.38	501.89
crystal system	orthorhombic	orthorhombic
space group	*Pbcn* (No. 60)	*Pna*2$_1$ (No. 33)
a [Å]	28.3122(3)	16.837(3)
b [Å]	14.2257(1)	10.2189(16)
c [Å]	13.7374(1)	9.0231(10)
V [Å^3]	5532.89(8)	1552.5(4)
Z	12	4
ρ_{calcd} [g cm^{-3}]	2.0506(1)	2.1473(6)
μ [mm^{-1}] ($Mo_{K\alpha}$)	9.28	9.35
F(000)	3216	960
crystal size [mm]	0.25 × 0.38 × 0.50	0.03 × 0.08 × 0.25
$(\sin\theta/\lambda)_{max}$ [Å^{-1}]	0.65	0.65
reflections collected	40529	11626,
unique reflections	6341	2166
R_{int}	0.086	0.106
transmission range	0.050–0.480	0.736–1.223
parameters/restraints	310/138	182/79
R_1[a]	0.0359	0.0350
wR_2[b]	0.095	0.0558
Goodness of fit	1.02	1.054
w^{-1}[c]	$\sigma^2(F_o^2) + (0.0415P)^2 + 8.5439P$	$\sigma^2(F_o^2) + (0.0146P)^2$
residual electron density [e Å^{-3}]	1.14/–0.98	0.97/–1.01

[a] $R_1 = \Sigma||F_O| - |F_C||/\Sigma|F_O|$, for all $I > 4\sigma(I)$. [b] $wR_2 = [\Sigma[w(F_o^2 - F_c^2)^2]/\Sigma[w(F_o^2)^2]]^{1/2}$. [c] $P = (\max(F_o^2,0) + 2F_c^2)/3$.

Acknowledgement

We thank Prof. Dr. R. van Eldik and Dr. H. C. Bajaj (kinetic experiments) and Prof. Dr. E. J. Baerends (bonding principles) for stimulating discussions. This work was supported in part (M.L. and A.L.S.) by the Netherlands Foundation for Chemical Sciences (C.W.) with financial aid from the Netherlands Organization for Scientific Research (N.W.O.).

[1] a) J. Lelieveld, J. Heintzenberg, *Science* **1992**, *258*, 117; b) R. J. Charlson, J. E. Lovelock, M. O. Andreae, S. G. Warren, *Nature* **1987**, *326*, 655; c) K. Capaldo, J. J. Corbett, P. Kasibhatia, P. Fischbeck, S. N. Pandis, *Nature* **1999**, *400*, 743; d) R. J. Charlson in, *The Changing Atmosphere* (Eds.: F. S. Rowland, I. S. A. Isaksen), Wiley, Chichester, **1988**, p. 79; e) M. O. Andreae in, *The Biogeochemical Cycling of*

Sulfur and Nitrogen in the Remote Atmosphere (Eds.: J. N. Galloway, R. J. Charlson, M. O. Andreae, H. Rohde), Reidel, Dordrecht, **1985**, p. 5; f) P. Brimblecombe, C. Hammer, H. Rohde, A. Ryaboshapko, C. F. Boutron in, *Evolution of the Global Biogeochemical Sulphur Cycle* (Eds.: P. Brimblecombe, A. Y. Lein), Wiley, NewYork, **1989**, p. 77; g) European Union, Agreement on the Reduction of Emissions of Fuels, June **1998**.

[2] a) J. R. Holum, *Elements of General and Biological Chemistry*, 4th ed., Wiley, New York, **1975**, p. 188; b) I. S. A. Isaksen in, *The Changing Atmosphere* (Eds.: F. S. Rowland, I. S. A.Isaksen), Wiley, Chichester, **1988**, p. 141.

[3] a) J. Janata, *Principles of Chemical Sensors*, Plenum, New York, **1989**; b) R. M. Crooks, A. J. Ricco, *Acc. Chem. Res.* **1998**, *31*, 219; c) J. Mitrovics, H. Ulmer, U. Weimar, W. Göpel, *Acc. Chem. Res.* **1998**, *31*, 307.

[4] a) P. Bühlmann, E. Pretsch, E. Bakker, *Chem. Rev.* **1998**, *98*, 1593; b) C. A. Daws, C. L. Exstrom, J. R. Sowa, K. R. Mann, *Chem. Mater.* **1997**, *9*, 363.

[5] a) K. Gleu, W. Breuel, K. Rehm, *Z. Anorg. Allg. Chem.* **1938**, *235*, 201; b) K. Gleu, W. Breuel, K. Rehm, *Z. Anorg. Allg. Chem.* **1938**, *235*, 211; c) K. Gleu, K. Rehm, *Z. Anorg. Allg. Chem.* **1936**, *227*, 237.

[6] a) G. J. Kubas, *Acc. Chem. Res.* **1994**, *27*, 183; b) W. A. Schenk, *Angew. Chem.* **1987**, *99*, 101; *Angew. Chem. Int. Ed. Engl.* **1987**, *26*, 98.

[7] a) D. M. P. Mingos, *Transition Met. Chem.* **1978**, *3*, 1; b) R. R. Ryan, G. J. Kubas, D. C. Moody, P. G. Eller, *Struct. Bonding* **1981**, *46*, 47; c) G. J. Kubas, *Inorg. Chem.* **1979**, *18*, 182; d) J. Reinhold, M. Schüler, T. Hoffmann, E. Wenschuh, *Inorg. Chem.* **1992**, *31*, 559; e) L. Vaska, *Acc. Chem. Res.* **1968**, *1*, 334.

[8] see for example: a) L. H. Vogt, J. L. Katz, S. E. Wiberley, *Inorg. Chem.* **1965**, *4*, 1157; b) R. R. Ryan, G. J. Kubas, *Inorg. Chem.* **1978**, *17*, 637; c) G. J. Kubas, G. D. Jarvinen, R. R. Ryan, *J. Am. Chem. Soc.* **1983**, *105*, 1883; d) E. H. Braye, W. Hübel, *Chem. Ber.* **1964**, *97*, 1871.

[9] see for example: a) S. J. La Placa, J. A. Ibers, *Inorg. Chem.* **1966**, *5*, 405; b) K. W. Muir, J. A. Ibers, *Inorg. Chem.* **1969**, *8*, 1921; c) T. E. Nappier, D. W. Meek, R. M. Kirchner, J. A. Ibers, *J. Am. Chem. Soc.* **1973**, *95*, 4194; d) P. G. Eller, R. R. Ryan, *Inorg. Chem.* **1980**, *19*, 142; e) U. Schimmelpfennig, R. Zimmering, K. D. Schleinitz, R. Stösser, E. Wenschuh, U. Baumeister, H. Hartung, *Z. Anorg. Allg. Chem.* **1993**, *619*, 1931.

[10] J. Terheijden, P. W. Mul, G. van Koten, F. Muller, H. C. Stam, *Organometallics* **1986**, *5*, 519.

[11] a) L. Vaska, S. S. Bath, *J. Am. Chem. Soc.* **1966**, *88*, 1333; b) R. R. Ryan, G. J. Kubas, *Inorg. Chem.* **1978**, *17*, 637.

[12] M. Albrecht, R. A. Gossage, A. L. Spek, G. van Koten, *Chem. Commun.* **1998**, 1003.

[13] J. H. Holtz, S. A. Asher, *Nature* **1997**, *389*, 829.

[14] J. A. M. van Beek, G. van Koten, M. J. Ramp, N. C. Coenjaarts, D. M. Grove, K. Goubitz, M. C. Zoutberg, C. H. Stam, W. J. J. Smeets, A. L. Spek, *Inorg. Chem.* **1991**, *30*, 3059.

[15] M. Albrecht, G. van Koten, *Adv. Mater.* **1999**, *11*, 171.

[16] a) G. van Koten, *Pure Appl. Chem.* **1989**, *61*, 1681; b) M. H. P. Rietveld, D. M. Grove, G. van Koten, *New. J. Chem.* **1997**, *21*, 751.

[17] For other applications of metallo-dendrimers, see for example: a) E. C. Constable, *Chem. Commun.* **1997**, 1073; b) M. A. Hearshaw, R. J. Moss, *Chem. Commun.* **1999**, 1; c) G. R. Newkome, E. He, C. N. Moorefield, *Chem. Rev.* **1999**, *99*, 1689.

[18] a) D. M. Grove, G. van Koten, J. N. Louwen, J. G. Noltes, A. L. Spek, H. J. C. Ubbels, *J. Am. Chem. Soc.* **1982**, *104*, 6609; b) J. Terheijden, G. van Koten, F. Muller, D. M. Grove, K. Vrieze, *J. Organomet. Chem.* **1986**, *315*, 401.

[19] C. J. Hawker, J. M. J. Fréchet, *J. Am. Chem. Soc.* **1990**, *112*, 7638.

[20] P. J. Davies, N. Veldman, D. M. Grove, A. L. Spek, B. T. G. Lutz, G. van Koten, *Angew. Chem.* **1996**, *108*, 2078; *Angew. Chem. Int. Ed. Engl.* **1996**, *35*, 1959.

[21] T. M. Miller, E. W. Kwock and T. X. Neenan, *Macromolecules* **1992**, *25*, 3143.

[22] P. J. Davies, D. M. Grove, G. van Koten, *Organometallics* **1997**, *16*, 800.

[23] J. C. Muijsers, J. W. Niemantsverdriet, I. C. M. Wehman-Ooyevaar, D. M. Grove, G. van Koten, *Inorg. Chem.* **1992**, *31*, 2655.

[24] I. Dance in, *The Crystal as a Supramolecular Entity* (Ed.: G. R. Desiraju), Wiley, Chichester, **1996**, p. 137.

[25] I. C. M. Wehman-Ooyevaar, G. M. Kapteijn, D. M. Grove, W. J. J. Smeets, A. L. Spek, G. van Koten, *J. Chem. Soc. Dalton Trans.* **1994**, 703.

[26] a) R. A. Gossage, L. A. van de Kuil, G. van Koten, *Acc. Chem. Res.* **1998**, *31*, 423; b) C. Granel, P. Dubois, R. Jérôme, P. Teyssié, *Macromolecules* **1996**, *29*, 8576.

[27] Furthermore, in all adduct complexes the satellite signals due to ^{195}Pt-^{1}H coupling are more clearly resolved upon addition of sulfur dioxide; see Supporting Information on the WWW under http://www.wiley-vch.de/home/chemistry/.

[28] Despite an earlier statement,[10] it is impossible to see both the SO_2 adduct and the free complex simultaneously by two sets of NMR signals at any concentration of sulfur dioxide.

[29] a) J. A. M. van Beek, G. van Koten, G. P. C. M. Dekker, E. Wissing, M. C. Zoutberg, C. H. Stam, *J. Organomet. Chem.* **1990**, *394*, 659; b) M. Oki, *Pure Appl. Chem.* **1989**, *61*, 699; c) M. Oki, M. Ohira, *Chem. Lett.* **1982**, 1267.

[30] a) A. Wojcicki, *Acc. Chem. Res.* **1971**, *4*, 344; b) F. Faraone, L. Silvestro, S. Sergi, R. Pietropaolo, *J. Organomet. Chem.* **1972**, *46*, 379; c) A. Wojcicki, *Adv. Organomet. Chem.* **1974**, *12*, 31; d) S. L. Miles, D. L. Miles, R. Bau, T. C. Flood, *J. Am. Chem. Soc.* **1978**, *100*, 7278; e) Y.-R. Hu, A. Wojcicki, M. Calligaris, G. Nardin, *Organometallics* **1987**, *6*, 1561.

[31] R. D. Shannon, C. T. Prewitt, *Acta Crystallogr. Sect. B* **1969**, *25*, 925.

[32] a) M. R. Snow, J. A. Ibers, *Inorg. Chem.* **1973**, *12*, 224; b) M. R. Snow, J. McDonald, F. Basolo, J. A. Ibers, *J. Am. Chem. Soc.* **1972**, *94*, 2526.

[33] The SO_2 molecule were rotated around the Pt–S axis in intervals of 3°. The energies of the conformationally minimalized structures (mm2 level) were calculated by extended Hückel methods with Alvarez collected parameters.

[34] a) J.-M. Lehn, *Supramolecular Chemistry: Concepts and Perspectives*, VCH, Weinheim, **1995**; b) C. B. Aakeroy, K. R. Seddon, *Chem. Soc. Rev.* **1993**, 397; c) J. C. MacDonald, G. M. Whitesides, *Chem. Rev.* **1994**, *94*, 2383; d) A. D. Burrows, C.-W. Chan, M. M. Chowdry, J. E. McGrady, D. M. P. Mingos, *Chem. Soc. Rev.* **1995**, 329; e) S. C. Zimmerman, F. Zeng, D. E. C. Reichert, S. V. Kolotuchin, *Science* **1996**, *271*, 1095.

[35] A similar network mediated by bridging SO_2 has been found in inorganic coordination compounds, see: M. Y. Darensbourg, T. Tuntulani, J. H. Reibenspies, *Inorg. Chem.* **1995**, *34*, 6287, but not in related platinum compounds containing NCN-type ligands, see for example, ref [10].

[36] W. J. J. Smeets, A. L. Spek, A. J. M. Duisenberg, J. A. M. van Beek, G. van Koten, *Acta Crystallogr. Sect. C* **1987**, *43*, 463.

[37] C. L. Young in, *Solubility Data Series*, *Vol. 12* (Ed.: C. L. Young), Pergamon, Oxford, **1983**, p. 145.

[38] In a previous report,[15] qualitatively different but incorrect data were presented for the equilibrium of dendritic **3** with SO_2.

[39] a) J. A. M. van Beek, G. van Koten, W. J. J. Smeets, A. L. Spek, *J. Am. Chem. Soc.* **1986**, *108*, 5010; b) R. A. Gossage, A. D. Ryabov, A. L. Spek, D. J. Stufkens, J. A. M. van Beek, R. van Eldik, G. van Koten, *J. Am. Chem. Soc.* **1999**, *121*, 2488.

[40] a) E. Lindner, M. Haustein, R. Fawzi, M. Steimann, P. Wegner, *Organometallics* **1994**, *13*, 5021; b) E. Lindner, M. Geprägs, K. Gierling, R. Fawzi, M. Steimann, *Inorg. Chem.* **1995**, *34*, 6106.

[41] a) D. F. Burow, *Inorg. Chem.* **1972**, *11*, 573; b) E. J. Woodhouse, T. H. Norris, *Inorg. Chem.* **1971**, *10*, 614; c) J. Jander, G. Tuerk, *Angew. Chem.* **1963**, *75*, 792; *Angew. Chem.* **1963**, *2*, 548.

[42] a) J. D. Childs, D. van der Helm, S. D. Christian, *Inorg. Chem.* **1975**, *14*, 1387; b) D. van der Helm, J. D. Childs, S. D. Christian, *J. Chem. Soc. Chem. Commun.* **1969**, 887.

[43] M. Berggren, A. Dodabalapur, R. E. Slusher, Z. Bao, *Nature* **1997**, *389*, 466.

[44] a) U. Kragl, C. Dreisbach, C. Wandrey, in *Applied Homogeneous Catalysis with Organometallic Compounds*, *Vol. 2* (Eds.: B. Cornilis, W. A. Herrmann), VCH, Weinheim, **1996**, p. 832.

[45] Molecular modeling (mm2 level) demonstrates a disk-like structure for **15** with a maximal Cl–Cl distance of 3.2 nm.

[46] J. S. Moore, *Acc. Chem. Res.* **1997**, *30*, 402.

[47] P. K. Byers, A. J. Canty, H. Jin, D. Kruis, B. A. Markies, J. Boersma, G. van Koten, *Inorg. Synth.* **1998**, *32*, 162.

0947-6539/00/0608-1444 $ 17.50+.50/0 *Chem. Eur. J.* **2000**, *6*, No. 8

[48] a) G. B. Kauffman, D. O. Cowan, *Inorg. Synth.* **1960**, *21*, 211; b) R. Roulet, C. Barbey, *Helv. Chim. Acta* **1973**, *56*, 2179; c) P. L. Goggin, R. J. Goodfellow, S. R. Haddock, F. J. S. Reed, J. G. Smith, K. M. Thomas, *J. Chem. Soc. Dalton Trans.* **1972**, 1904.
[49] A. L. Spek, *J. Appl. Crystallogr.* **1988**, *21*, 578.
[50] A. L. Spek, *Acta Crystallogr. Sect. A* **1990**, *46*, C34.
[51] P. T. Beurskens, G. Admiraal, G. Beurskens, W. P. Bosman, S. Garcia-Granda, R. O. Gould, J. M. M. Smits, C. Smykalla, *The DIRDIF Program System. Technical Report of the Crystallography Laboratory*, University of Nijmegen (The Netherlands), **1992**.
[52] G. M. Sheldrick, *SHELXL-96 Program for Crystal Structure Refinement*, *Beta test version*, University of Göttingen (Germany), **1996**.

Received: August 23, 1999 [F1998]